Title: Scale-invariance in brain activity predicts practice effects in cognitive performance

Authors: Omid Kardan[1], Elliot Layden[1], Kyoung Whan Choe[1], Muxuan Lyu[2], Xihan Zhang[1], Sian L. Beilock[3], Monica D. Rosenberg[1], & Marc G. Berman[1]

[1]University of Chicago, Chicago, IL, USA

[2]The Hong Kong Polytechnic University, Hong Kong

[3]Barnard College, Columbia University, NY, USA

Address correspondence to Omid Kardan okardan@uchicago.edu, or Marc G. Berman bermanm@uchicago.edu

Abstract

Although practicing a task generally benefits later performance on that same task ('practice effect'), there are large—and mostly unexplained—individual differences in reaping the benefits from practice. One promising avenue to model and predict such differences comes from recent research showing that brain networks can extract functional advantages from operating in the vicinity of criticality, a state in which brain network activity is more scale-free. As such, we hypothesized that individuals with more scale-free fMRI activity, indicated by BOLD time series with a higher Hurst exponent (*H*), gain more benefits from practice. In this study, participants practiced a test of working memory and attention, the dual *n*-back task (DNB), watched a video clip as a break, and then performed the DNB again, during MRI. To isolate the practice effect, we divided the participants into two groups based on improvement in performance from the first to second DNB task run. We identified regions and connections in which *H* and functional connectivity related to practice effects in the last run. More scale-free brain activity in these regions during the preceding runs (either first DNB or video) distinguished individuals who showed greater DNB performance improvements over time. In comparison, functional connectivity (r^2) in the identified connections did not reliably classify the two groups in the preceding runs. Finally, we replicated both *H* and r^2 results from study 1 in an independent fMRI dataset of participants performing multiple runs of another working memory and attention task (word completion). We conclude that the brain networks can accommodate further practice effects in individuals with higher scale-free BOLD activity.

Introduction

Improvements in cognitive test performance due to repeated practice considerably vary across individuals, even within the same test (Calamia et al, 2012). When situational factors and age are controlled for, the variability observed in these so called 'practice effects' (see McCaffrey, Duff, & Westervelt, 2000) across healthy individuals is traditionally attributed to differences in intellectual ability, where individuals with higher fluid intelligence benefit more from practice (Rapport et al, 1997). The magnitude of practice effects in multiple tests of working memory, attention, and executive function has been shown to provide rich and unique information about the respondent for diagnosis of clinical conditions as well as their responsiveness to interventions (Duff et al, 2012). Given the diagnostic and prognostic values of practice effects, it is important to pursue mechanistic models for explaining individual differences in learning from practice (i.e., move beyond the less specific 'the rich get richer' argument), and hone in on a neuropsychological model of individuals' future task improvement based on the state of their brain activity. In the current study, we characterize the brain as a network that imparts functional advantages when operating in the vicinity of *criticality*. We show that brain network criticality provides a theoretical framework for investigating multiple aspects of cognitive performance, including whether or not one is likely to improve over time in a working memory and attention task.

A common way to measure the criticality of large-scale brain networks (see Box 1) is via estimation of time scale-invariance (e.g., the $1/f$ component of power spectral density function) in brain activity. Specifically, scale-free brain activity has been successfully measured using the Hurst exponent (H) for both electrophysiological brain activity (e.g., EEG, MEG, ECoG) and blood-oxygen-level-dependent (BOLD) fMRI signals, where higher H indicates more scale-free dynamics. H in electrophysiological and fMRI signals has been shown to be suppressed during the exertion of cognitive effort (Churchill et al., 2016; He, 2014; Kardan, Adam, et al., 2020), following sport-related concussions (Churchill et al., 2020), and with distress and aging (Churchill et al., 2016; Goldberger et al., 2002). For example, Kardan et al. (2020) found that when individuals were performing a task with trials of low, medium, or high working memory demands, global suppression of H in EEG brain activity tracked the task loads, concluding that lowered H is indicative of a departure from the state of rest towards an 'effortful' state (i.e., further away from criticality). Notably, the degree of H suppression monotonically tracked task demands within individuals better than specific EEG oscillatory components. Given this modulation of H with cognitive exertion, we hypothesized that individual differences in average H of whole-brain activity when performing equally well on a task

could signal differences in the potential for further improvement in the task. Improving performance in non-trivial tasks generally requires efficient implicit and explicit learning of task characteristics and forming better task-relevant memories and cognitive strategies. Our hypothesis is that higher H would accommodate cognitive resources for such processes.

Box 1. Critical state in a dynamic network

Consider a physical system whose large-scale behavior is not merely the sum of its smaller components (i.e., it is a network with interactions between nodes). Such system can be in different states based on whether the network configuration is poised at minimum stability or not. As a toy example, the network in Figure 1 consists of nodes with active or inactive states, where network dynamics are configured such that an active node becomes inactive at the rate of λ, and activity in a node spreads to a random neighboring inactive node at the rate of γ. In such network, the time evolution of a small scale local activity can be spread chaotically if $\lambda < \gamma$ or be absorbed before resulting in global activity patterns if $\lambda > \gamma$. At the border between these two regimes ($\lambda = \gamma$), the observed global patterns of activity tend to become self-similar over different temporal or spatial scales, i. e., scale-invariant, as they follow the power-law distribution (Frette et al., 1996; Muñoz, 2018). In other words, this 'critical' state ($\lambda = \gamma$) separates the subcritical phase ($\lambda > \gamma$), where transient activity decays to a zero-activity steady state, from the supercritical phase ($\lambda < \gamma$), where transient activity turns into sustained global activity. Therefore, the minimal stability of the network at critical state enables maximum susceptibility to perturbation by environmental inputs while avoiding sustained global activity that prevents sensitivity to other transient activity (Chialvo, 2004; Fraiman, Balenzuela, Foss, & Chialvo, 2009; Frette et al., 1996). One can conceive of brain networks similarly: small-scale neuronal ensembles with short- and long-term interactions (phase-coupled electro-chemical activity) give rise to the emergent large-scale activity linked to cognitive functions (Chialvo, 2010; Cocchi, Gollo, Zalesky, & Breakspear, 2017; Fagerholm et al., 2015; Gisiger, 2001; He, 2014; Werner, 2010). There is evidence of self-organized criticality in the human brain's intrinsic activity (de Arcangelis, Perrone-Capano, & Herrmann, 2006; Kitzbichler, Smith, Christensen, & Bullmore, 2009), permitting dynamic reorganization into alternative states (i.e., further from criticality) depending on behavioral and cognitive demands (Arviv, Goldstein, & Shriki, 2015; Fagerholm et al., 2015; Hahn et al., 2017; Yu et al., 2017).

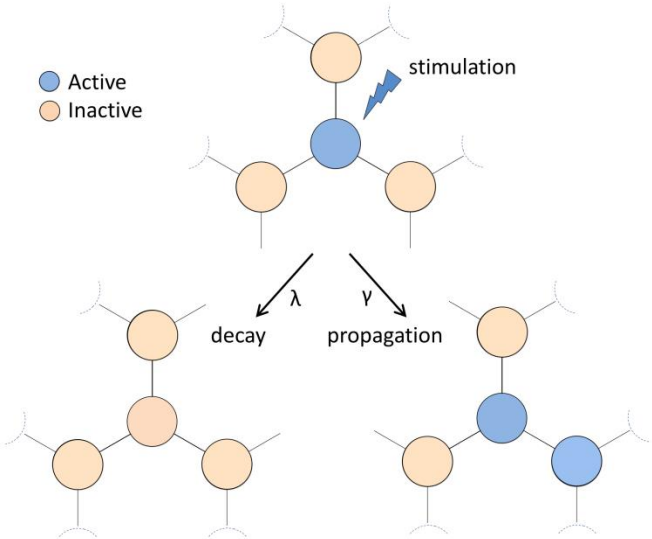

Figure 1. Schematic of dynamics of de-activation of an active node or propagation of activity to a neighboring node in a simple network exhibiting non-equilibrium phase transition. Different relationship between activation rate (γ) and deactivation rate (λ) results in the network to be in subcritical, critical, or supercritical state.

In simulated neural networks, operating at critical state has been shown to provide multiple advantageous functional properties for the network such as improved information storage and transfer (Boedecker, Obst, Lizier, Mayer, & Asada, 2012; Shriki et al., 2013; Shriki & Yellin, 2016; Tanaka, Kaneko, & Aoyagi, 2008) and dynamic range (Gautam, Hoang, McClanahan, Grady, & Shew, 2015; Kinouchi & Copelli, 2006). Operating near criticality may also facilitate learning and plastic adaptation (de Arcangelis & Herrmann, 2010). In our proposed framework, *H* is a measure that indicates brain network proximity or departure from criticality (Kardan et al., 2020). Under our hypothesis, the temporal and spatial efficiency of information transfer between the nodes of brain networks is diminished when *H* is low. For example, when an exogenous task demand suppresses *H*, the ability to process other exogenous or endogenous cognitive demands is diminished due to the transition to a sub-critical state. Therefore, between two individuals initially performing equally well in a working memory and attention test, the person with higher *H* while performing the task is likely enjoying more efficient information processing (as if performing an easier task despite the apparent equal performance). Our hypothesis is that such advantage will eventually emerge as higher performance in the task the second time around, because efficient information processing facilitates any *additional* processes required for *improving* the execution of task. Since this advantage resulting in disproportionate gain in later performance (compared to the lower *H* individual) need not be immediately apparent in initial behavioral performance, this proposed hypothesis could provide an avenue to model practice effects in a predictive manner.

In the current study, participants performed an audio-visual dual *n*-back (DNB) task (Jaeggi, Buschkuehl, Jonides, & Perrig, 2008) two times, with an intermission video in between as a rest break. We divided the participants into two groups based on pure improvement in DNB performance (i.e., adjusted for baseline performance). Our hypothesis was that participants with higher *H* would show greater improvements in DNB performance from run 1 to run 2. We identified regions in which *H* related to practice effects in the last run, and showed higher average *H* during either the first DNB run or the video break run in those regions is sufficient for distinguishing task improvers from non-improvers. Additionally, we identified functional connections in the last run whose strength related to practice effects, and showed that the strength of these connections during either the first DNB run or the video run did not distinguish improvers from non-improvers, demonstrating that not *any* brain activity measure related to task performance can distinguish the two groups. Finally, we replicated our results of study 1 by showing that higher average *H* in the regions identified in study 1 successfully distinguished improvers from non-improvers in an independent dataset with a different repeated cognitive test of working memory and attention

(word completion task, study 2). In summary, we propose that differences in scale-invariance of fMRI BOLD activity can characterize individual differences in practice effects.

Results

Behavioral results in study1: Improvers vs. non-improvers

For each fMRI run, task performance was operationalized as discrimination index A' averaged across all 6 DNB task blocks. There was an average improvement of ΔA' = 0.045 in performance (i.e., 5.5% improvement) from first run of dual *n*-back (A'_0; Mean = 0.827, SD = 0.081) to dual *n*-back run 2 (A'_f; Mean = 0.872, SD = 0.081), with large variability in the amount of change in performance (ΔA') across individuals (SD = 0.045; Figure 2). Linear regression of ΔA' on video type and preference rating for the video failed to find a significant relationship between video type or video rating and change in performance (t = 0.403, p = 0.688 for video type and t = -0.870, p = 0.388 for preference rating). Therefore, we collapsed the participants on the video types for the rest of the analyses.

All performance levels (shown in figure 2) were above chance (i.e., A'>0.5), suggesting that participants were engaged and compliant during the DNB runs. Importantly, we wanted to assess practice effects independent of baseline performance in our fMRI based classification models. To do this, we regressed A'_0 out of ΔA' to make *adj.* ΔA' scores that are linearly independent from baseline performance. We then split the participants into improvers and non-improvers based on a median split of *adj.* ΔA' (Figure 2 blue vs. red lines). When using adj. ΔA', there was no significant difference between the baseline performance of the two groups (A'_0 = 0.836 for non-improvers and 0.818 for improvers, t = 0.838, p = 0.405), but improvers had significantly higher performance the second time around compared to non-improvers (A'_f = 0.846 for non-improvers and 0.898 for improvers, t =2.528, p = 0.014). Although our main analysis involves the adjusted ΔA', we also performed an additional classification with improvers vs. non-improvers defined based on a median split of ΔA' non-adjusted for baseline performance and replicated the same findings (see supplementary Figure S1).

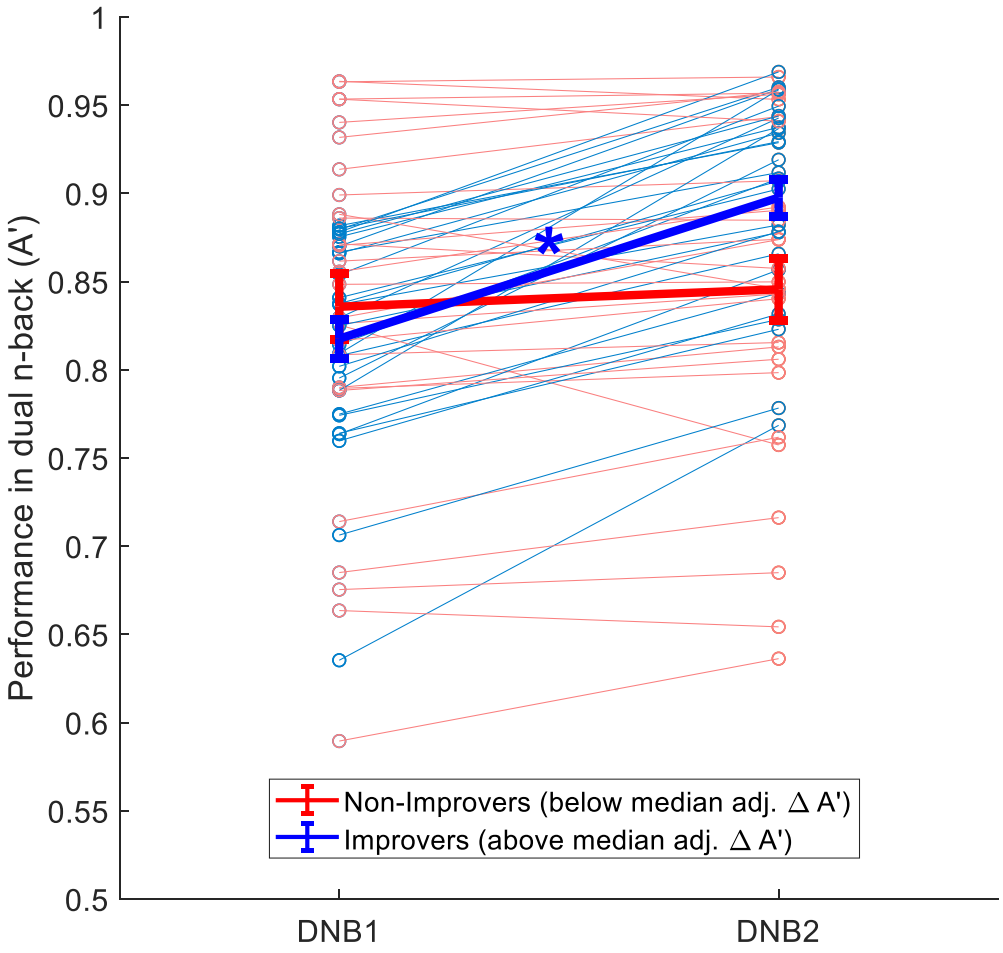

Figure 2. Performance in the dual *n*-back task in all participants color-coded by change in performance for improvers (blue) and non-improvers (red). When change in performance was residualized with baseline performance the defined improvers and non-improvers on average started equally well, but improvers had significantly higher performance in the second dual n-back run. Error bars show ±SE.

fMRI results in study1: Defining regions and functional connections of interest

In addition to evaluating global average *H* and r^2 across the whole brain (see Methods), we also selected a subset of voxel-level regions of interest (ROI) and a subset of functional connections of interest (COI) from the *H* and r^2 whole-brain data that were most relevant in distinguishing the performance from improvers and from non-improvers in the dual *n*-back task. We used the fMRI data from the 2nd dual n-back run to define the ROIs and COIs. No brain data from the first two runs

(first dual *n*-back and video) were used in the ROI or COI selection, as these data were set aside for subsequent classification analyses. The selection of the subset of voxels for classification analysis (i.e., the ROI) and subset of connections for classification analysis (i.e., the COI) was done based on whether a voxel's *H* or a functional connection's r^2 had a correlation above $\rho > 0.25$ with *adj*. ΔA' (i.e., at least a small association size (Kirk, 2012) between variables), and whether that condition was met in more than half of data bootstraps (total of 200 resamples with replacement)[1]. Figure 3A shows these voxels and figure 3B shows the connections which comprised of 5409 voxels (~8.5% of total) and 2747 pairwise connections (~3.6% of total), respectively. The ROI voxels fell mainly within the frontal and temporal lobes, and the COI connections mainly involved the temporal and frontal lobes, as well as the cerebellum. The full list of brain structures and their extent of overlap with the Hurst ROIs and the r^2 COIs are presented in supplementary Tables S1 and S2.

[1] The classification results are not dependent on this particular choice of threshold. For example for choices of $\rho > 0.15$ or $\rho > 0.35$, even though the sparsity of included voxels or connections in the ROI and COI change, the classification performances remain similar.

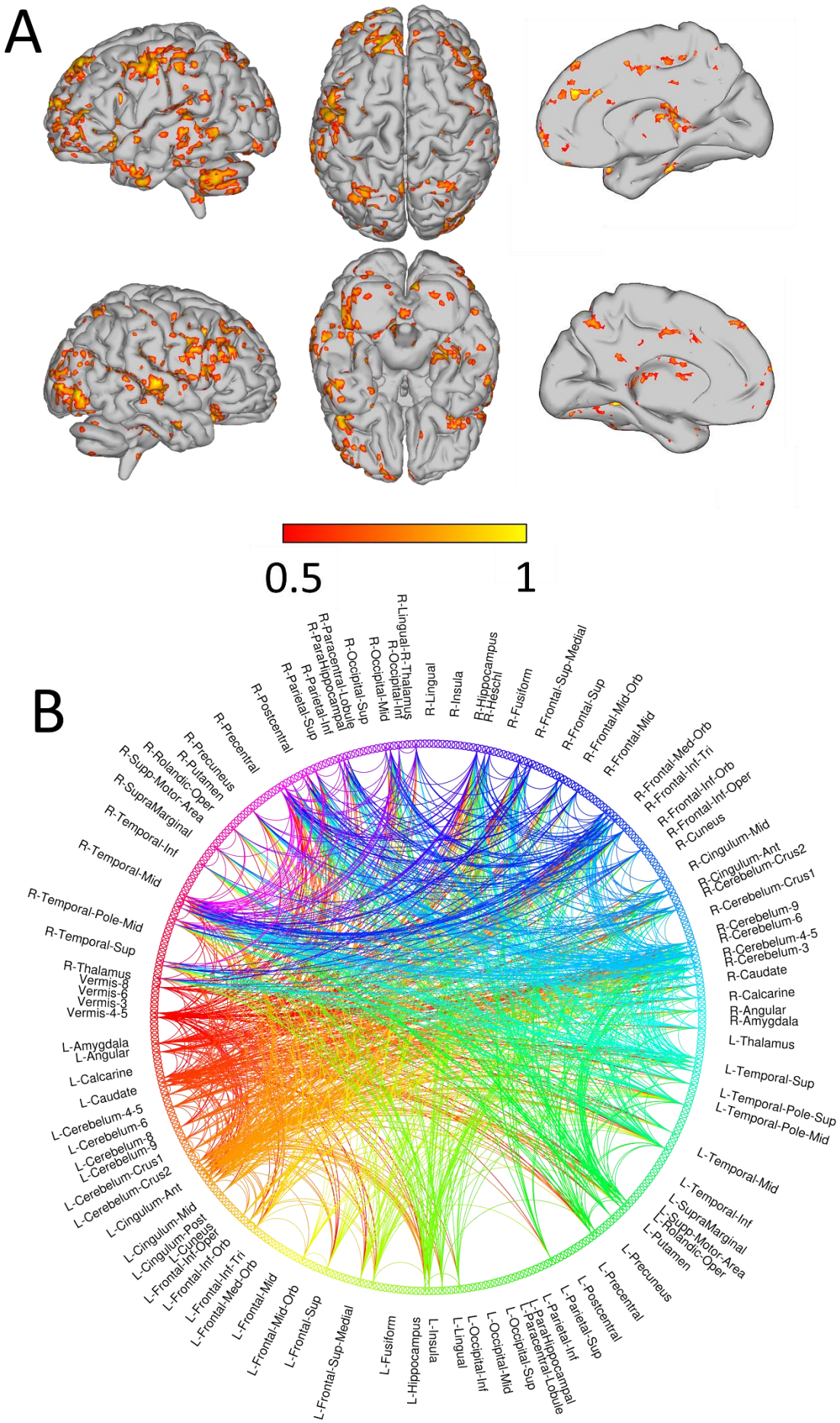
A
0.5
1
B
R-Lingual-R-Thalamus
R-Occipital-Inf
R-Occipital-Mid
R-Occipital-Sup
R-Paracentral-Lobule
R-ParaHippocampal
R-Parietal-Inf
R-Parietal-Sup
R-Postcentral
R-Precentral
R-Precuneus
R-Putamen
R-Rolandic-Oper
R-Supp-Motor-Area
R-SupraMarginal
R-Temporal-Inf
R-Temporal-Mid
R-Temporal-Pole-Mid
R-Temporal-Sup
R-Thalamus
Vermis-8
Vermis-6
Vermis-3
Vermis-4-5
L-Amygdala
L-Angular
L-Calcarine
L-Caudate
L-Cerebelum-4-5
L-Cerebelum-6
L-Cerebelum-8
L-Cerebelum-9
L-Cerebelum-Crus1
L-Cerebelum-Crus2
L-Cingulum-Ant
L-Cingulum-Mid
L-Cingulum-Post
L-Cuneus
L-Frontal-Inf-Orb
L-Frontal-Inf-Tri
L-Frontal-Med-Orb
L-Frontal-Mid
L-Frontal-Mid-Orb
L-Frontal-Sup
L-Frontal-Sup-Medial
L-Fusiform
L-Hippocampus
L-Insula
L-Lingual
L-Occipital-Inf
L-Occipital-Mid
L-Occipital-Sup
L-Paracentral-Lobule
L-ParaHippocampal
L-Parietal-Inf
L-Parietal-Sup
L-Postcentral
L-Precentral
L-Precuneus
L-Putamen
L-Rolandic-Oper
L-Supp-Motor-Area
L-SupraMarginal
L-Temporal-Inf
L-Temporal-Mid
L-Temporal-Pole-Mid
L-Temporal-Pole-Sup
L-Temporal-Sup
L-Thalamus
R-Amygdala
R-Angular
R-Calcarine
R-Caudate
R-Cerebelum-3
R-Cerebelum-4-5
R-Cerebelum-6
R-Cerebelum-9
R-Cerebelum-Crus1
R-Cerebelum-Crus2
R-Cingulum-Ant
R-Cingulum-Mid
R-Cuneus
R-Frontal-Inf-Oper
R-Frontal-Inf-Orb
R-Frontal-Inf-Tri
R-Frontal-Med-Orb
R-Frontal-Mid
R-Frontal-Mid-Orb
R-Frontal-Sup
R-Frontal-Sup-Medial
R-Fusiform
R-Heschl
R-Hippocampus
R-Insula
R-Lingual

Figure 3. The selected ROIs (A) and COIs (B) are illustrated here. **A.** The main clusters of the Hurst ROIs are located in the frontal and temporal lobes. The colorbar shows proportion of re-samples where the voxel passed the $\rho > 0.25$ with *adj*. ΔA', with threshold at 50%. **B.** The nodes with most connections in the r^2 COI (that passed the $\rho > 0.25$ with *adj*. ΔA') involve temporal and frontal regions, as well as cerebellum. For the full list of regions and connections see supplementary Tables S1 and S2.

fMRI results in study1: Scale-invariance distinguishes improvers in the dual n-back task

The classification of improvers vs. non-improvers within the dual *n*-back sample was successful using either average *H* in the ROI during the baseline/1st dual *n*-back run (i.e., H_{DNB1}) or average *H* in the ROI during the video viewing run (i.e., H_{Vid}), with both having class prediction accuracies of 64% and significantly better than the null classification distribution ($p = 0.025$ and $p = 0.005$ for H_{DNB1} and H_{Vid}, respectively). In comparison, the average r^2 values in the COIs during the baseline dual *n*-back ($Conn_{DNB1}$) or average r^2 in the COI during the video viewing run ($Conn_{Vid}$) failed to classify improvers from non-improvers significantly better than the null model, with respective accuracies of 53% and 57%.[2] The distribution for all classification bootstraps and their respective confusion matrices are shown in Figure 4 panels A and B.

There was a chance in the previous analysis that the H_{DNB1} model was capitalizing on the fact that the behavioral performance from the DNB1 run of the left-out participants were used in making the median split of improvers and non-improvers (i.e., regressing A'_0 out of ΔA' included all subjects' behavioral data). Therefore, we also used the fMRI data from only the video run (i.e., H_{Vid} or $Conn_{Vid}$) to predict improvers and non-improvers regardless of their baseline performance (i.e., where the median split was done on ΔA' non-adjusted for baseline performance). We repeated the classification procedure using the H_{Vid}, $Conn_{Vid}$, or the baseline performance to distinguish the new split of improvers and non-improvers that does not adjust for baseline performance and using fMRI data that does not include performing a task. The results showed similar prediction accuracy of 64% ($p = 0.025$) for H_{Vid}, while neither $Conn_{Vid}$ nor baseline performance have classification accuracies significantly better than chance (57% and 58%, respectively). Additionally, we used all three variables (A'_0, H_{Vid}, and $Conn_{Vid}$) and their two-way interactions for classification and left each variable out to observe the drops in prediction accuracy. This analysis showed that $Conn_{Vid}$ was completely redundant in the full model (i.e., no accuracy drops absent of $Conn_{Vid}$), and the best

[2] Separate analysis of negative and positive functional connectivity values (rather than r^2) resulted in slightly worse performance for the connectivity-based classifications.

classification model was one that included H_{Vid}, A'_0, and their two-way interaction, which performed at 70% accuracy. The classification accuracy distributions and confusion matrices for these analyses with non-adjusted ΔA' are shown in supplementary Figure S1.

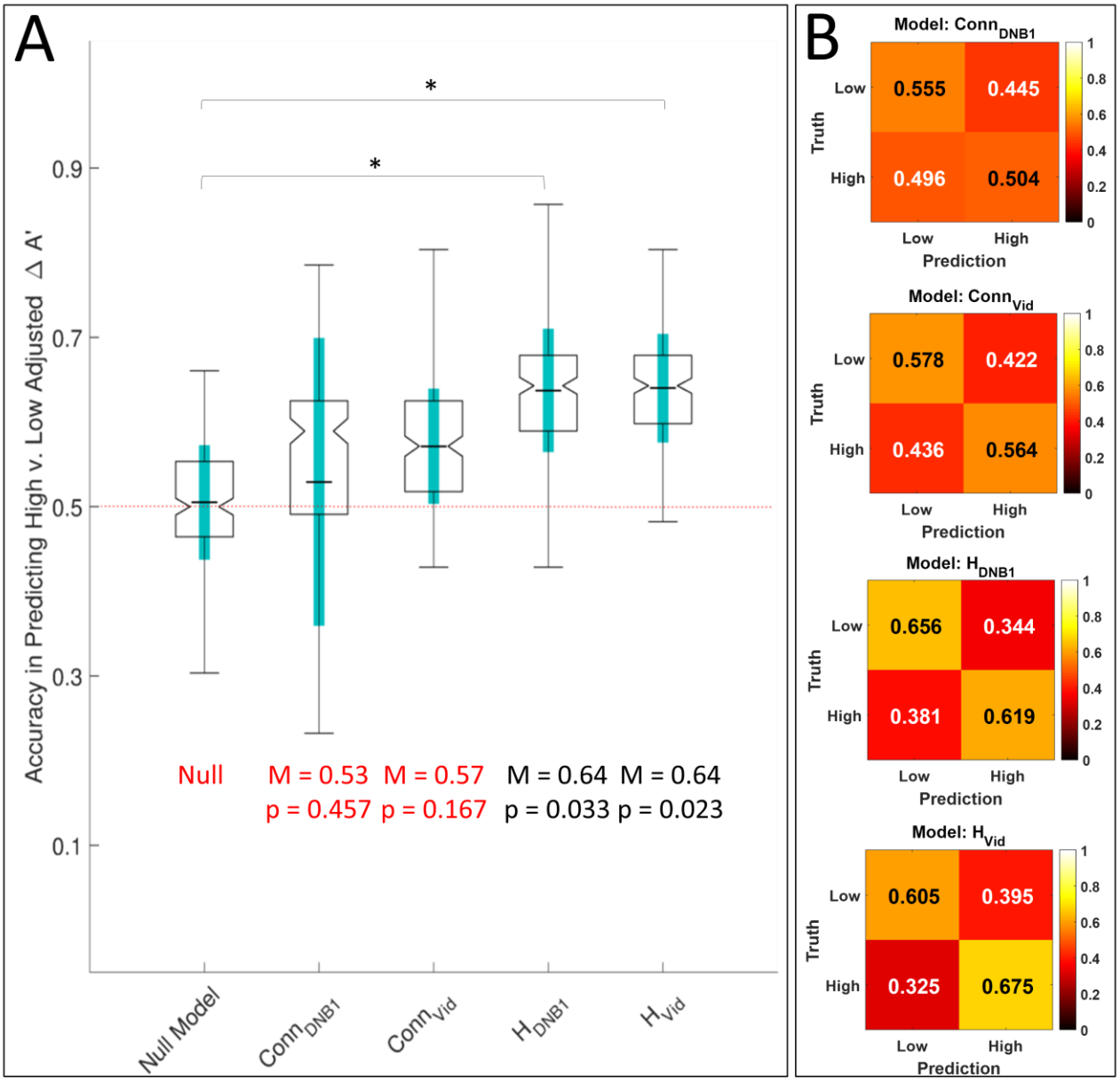

Figure 4. Classification accuracy distributions and confusion matrices for improvers and non-improvers (based on median split of adj. ΔA') are plotted in panel **A**, with corresponding confusion matrices shown in panel **B**. In panel A, each box-plot shows all the distribution of accuracies using the model indicated on the x-axis. The p values compare the null model distribution with models containing the variable indicated on the *x*-axis. M shows mean of the distribution of accuracies (so do black horizontal ticks inside the boxes), notch in the boxes show medians of distributions, and thick teal vertical lines show the SD of distributions around the means. The boxes show ±1 quantile

around the median and whiskers show range of the distribution. All statistics reported included all 1,000 bootstrap sample accuracies. In panel B, rows show true labels of the classes of improvers (labeled high) and non-improvers (labeled low), and columns show predicted labels. In confusion matrices higher values in main diagonals indicate better classification, while higher values off main diagonals indicates proportion of misclassified individuals.

fMRI results in study1: Higher H for improvers in the dual n-back task

To investigate whether the *H* signal distinguishing improvers from non-improvers was consistently higher for the improvers across the entire experiment (as we would hypothesize), we plotted average *H* across the whole brain and also within the selected ROIs across the three runs of the experiment for improvers and non-improvers (Figure 5 panels A and B, respectively). Even before ROI specification, we noted a trend toward higher global *H* averaged over all runs for improvers compared to non-improvers ($t = 1.99$, $p = 0.052$). This trend was considerably more pronounced after ROI selection (Figure 5B), which allowed for the successful classification of improvers and non-improvers presented earlier. Additionally, both global *H* and ROI *H* are higher during the video run compared to the dual *n*-back runs, irrespective of performance improvement ($t = 4.19$, $p < 0.001$ for global *H* and $t = 4.12$, $p < 0.001$ for ROI *H*). This replicates previous findings showing global *H suppression* with increased cognitive effort and task difficulty in fMRI and EEG data (Churchill et al., 2016; Kardan, Adam, et al., 2020). Figure 5B shows that ROI selection using the third run (DNB2) successfully increased the *H* distinction between the improvers and non-improvers in a manner that generalizes to runs prior to it. In contrast, the distinction created by COI selection for functional connectivity strength did not generalize to previous runs (Figure 5 panels C and D). This result indicates that the feature selection approach used did not bias the cross-validation results for the *H* model, given that the same approach was used for the r^2 based model.

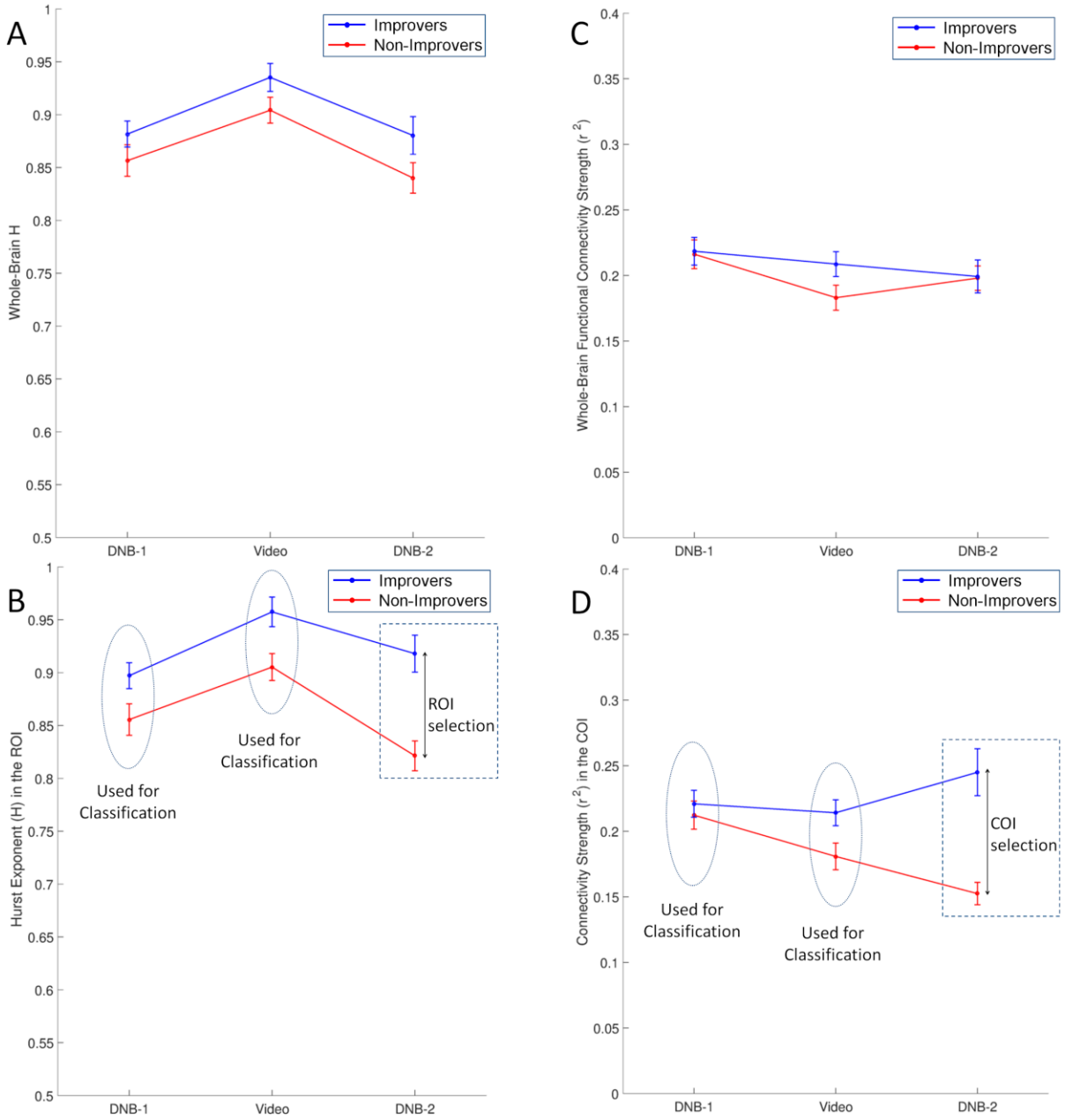

Figure 5. The average *H* (left panels) and average r^2 (right panels) for improvers and non-improvers. The *H* values are averaged over the whole brain in panel **A** and over the ROIs depicted in Figure 3A in panel **B**. The r^2 values are averaged over all pairwise connections in panel **C** and over the COIs depicted in Figure 3B in panel **D**. Errorbars show ±SE.

Study 2: Replication of H-based ROI results in word completion task

We used fMRI data from an independent sample of 45 participants to classify task improvers from non-improvers in a different cognitive test, the word completion task (as part of a

Choose-and-Solve Task (CAST; Choe et al., 2019), see *methods*). The performance levels of participants are shown in Figure 6, and panel B shows the performance separately for the two groups of improvers and non-improvers. The two groups were made similarly as in the dual *n*-back dataset, where a median split in change in performance between the last and the first run, adjusting for the baseline performance (i.e., adj. *Δ Performance*), determined the dichotomy for classification. The average *H* in the pre-defined ROI from our dual *n*-back dataset was calculated for each participant, and the mean values for each group (improvers and non-improvers) are plotted in Figure 6 panel C. Again, the direction of the distinction followed our hypothesis that individuals with higher *H* improved more in subsequent repetitions of the task, although the *H* difference between groups was only marginally significant ($F(1,43) = 3.99$, $p = 0.052$).

We used the *H* in the pre-defined ROI from dual *n*-back study in earlier runs of the word completion task (1, 2, and 3) to classify the improvers and non-improvers with leave-one-out linear discriminant (LD) classification similar to dual *n*-back dataset to replicate our results in an independent dataset and cognitive test. Since we only have one feature for classification, this step is simply comparing the left-out subject's *H* with mean *H* of left-in improvers and non-improvers, with similar bootstrapping and permutation procedure as before (see Methods *Classification of improvers vs. non-improvers using ROI and COI average H or* r^2). Utilizing the *H* from the first 3 runs (out of 6) was sufficient for the classifier to successfully distinguish eventual improvers from non-improvers above chance (63% accuracy, $p = 0.011$ compared to null distribution). Using only *H* in runs 1 and 2 did not classify the improvers from non-improvers significantly better than chance (59% accuracy, $p = 0.075$ compared to null distribution), though was numerically in our hypothesized direction. Figure 6D summarizes these classification results.

Importantly, there was no difference in reaction time to attention check trials in the word completion task between the improvers and non-improvers (965 ms for non-improvers vs. 956 ms for improvers, $t = 0.135$, $p = 0.893$), ruling out any potential differences in level of task engagement between the two groups. Lastly, classification of improvers vs. non-improvers based on the connectivity strength r^2 using the COI from dual *n*-back experiment failed to perform better than chance using the first three runs of word completion (and even when using all 6 runs) which was expected.

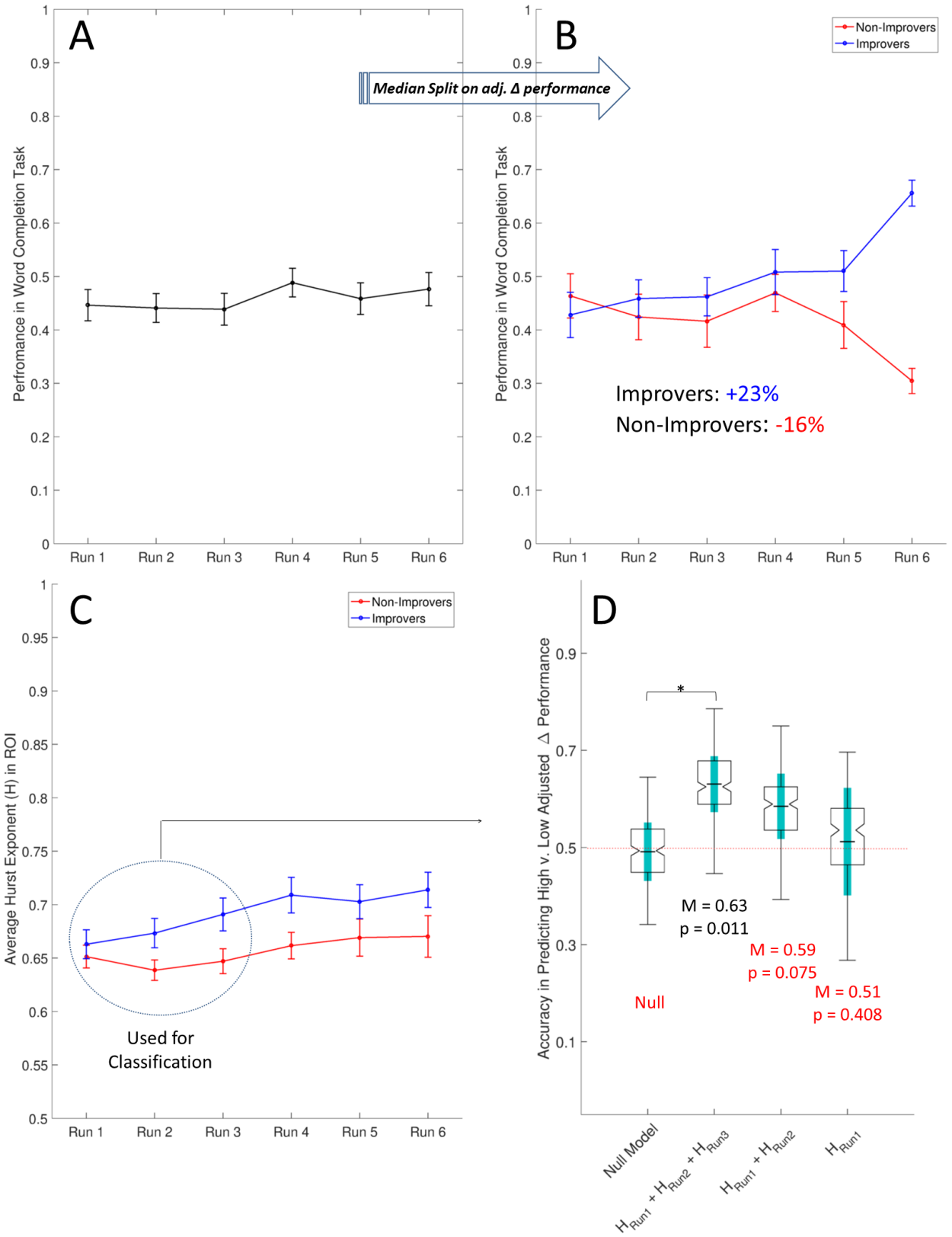
A
B
Median Split on adj. Δ performance
Non-Improvers
Improvers
Performance in Word Completion Task
Improvers: +23%
Non-Improvers: -16%
Run 1
Run 2
Run 3
Run 4
Run 5
Run 6
C
Average Hurst Exponent (H) in ROI
Used for Classification
D
Accuracy in Predicting High v. Low Adjusted Δ Performance
*
M = 0.63
p = 0.011
M = 0.59
p = 0.075
M = 0.51
p = 0.408
Null
Null Model
$H_{Run1} + H_{Run2} + H_{Run3}$
$H_{Run1} + H_{Run2}$
H_{Run1}

Figure 6. Behavioral performance in word completion task across runs (A), and separated by improvers vs. non-improvers groups (B). The *H* in the pre-defined ROI from the dual *n*-back experiment over all runs are shown in panel (C). Panel (D) shows classification accuracy boxplots of LD classifier with leave-one-participant-out cross-validation using the variable(s) indicated on the x axis. The p values compare each model with the null distribution, and thick vertical green lines indicate SD around the mean of distributions.

Discussion

Across two datasets with different cognitive tasks, individual differences in scale-free dynamics of the BOLD signal reliably predicted variability in cognitive task improvement. Higher *H* of fMRI activity successfully distinguished task improvers from non-improvers, adjusted for baseline task performance, in both datasets. Taken together, these findings provide evidence for utilizing scale-free dynamics of brain activity as an objective measure to predict who will benefit the most from practice in cognitive tasks.

Performing most complex tasks that engage working memory and focused attention require a degree of switching between sub-tasks and alterations in the locus of attention (Awh & Jonides, 2001; Ikkai & Curtis, 2011). Both of those processes depend on active information storage and transfer in neuronal ensembles. Research on neural networks has shown that criticality optimizes a number of such computationally advantageous properties (Beggs John M, 2008; Shew & Plenz, 2013, Boedecker et al., 2012; Shriki et al., 2013; Shriki & Yellin, 2016; Tanaka et al., 2008), in addition to the dynamic range of the network (Gautam et al., 2015; Kinouchi & Copelli, 2006). Let us assume that the observed fMRI scale-invariance differences between improvers and non-improvers in the current study delineate states of proximity or distance from criticality in brain networks (Kardan et al., 2020; see Muñoz, 2018 for other concepts in biology also termed as criticality and von Wegner, Laufs, & Tagliazucchi, 2018 for other interpretations of scale-free brain activity). Conceptualized in this way, we can then have a state-based or trait-based interpretation of our findings.

The state-based interpretation is that individuals who happened to be in a higher *H* state at the time of experiment processed the tasks more efficiently, leaving cognitive resources required for *additional* learning of task characteristics and forming better task-relevant memories and cognitive strategies. The encoding of these additional task-relevant information then enabled these individuals (i.e., improvers) to perform better the second time around.

The trait-based interpretation can be made in two related, but not equivalent ways. First, the tasks utilized here demanded less cognitive effort from improvers (i.e., less suppression of *H*, Kardan et al., 2020) due to them having higher fluid intelligence or working-memory capacity, which is in line with the neural efficiency intelligence hypothesis (Neubauer & Fink, 2009a & 2009b). This means that lower *H* during tasks for non-improvers could be due to them exerting more cognitive effort. As such lower/higher *H* is not a cause for less/more performance improvements, but a consequence of individuals being in different states of effort exertion. This account, however, does not explain the lower *H* observed in non-improvers even during the video run (i.e., when there is no overt task) for the dual *n*-back experiment. The other trait-based account is that improvers may have a more critically-organized functional brain network at baseline due to trait-level characteristics (e.g., maybe individuals with higher WM capacity or IQ are more frequently/consistently in more scale-free states). These individuals then have consistently higher *H* than others, even when not performing a task (e.g., during the video watching runs). Their higher *H* during cognitive tasks then enable them to more readily improve their performance due to advantages of criticality discussed before (He, 2011; Kitzbichler et al., 2009; Proekt, Banavar, Maritan, & Pfaff, 2012).

Importantly, the differences in *H* between individuals could also result from interactions of both trait- and state-level fluctuations in cognitive capabilities. Until further research reveals long-term stability of *H* in individuals, both possibilities (and their interaction) should be considered. Therefore, individual differences in *H* should not be deemed as indicators of trait measures of intelligence and intellectual ability alone. In fact, we believe it to be highly likely that both trait and state factors are contributing to differences in *H* and resulting changes in performance.

We also compared our *H*-based model's classification performance with that of a functional connectivity strength measure with similar feature selection and model training steps. This analysis was performed to test the specificity of our model, ensuring it was not the case that *any* measure describing brain network activity would yield the same level of classification accuracy. Our results indicated that *H*, but not r^2, predicted improvement from practice. Nevertheless, further comparisons between *H*-based models and functional connectivity-based models could be illuminating. Functional connectome-based models currently capitalize on diverse patterns of statistical dependencies between brain regions that are difficult to comprehensively integrate within a single theoretical framework. A strength of *H* is that it comes with a rich theoretical framework related to the efficiency of information transfer and criticality. Recent work is

beginning to link *H* and functional connectivity based models to each other and to predictors of behavior (Stier et al., in preparation).

There are a number of limitations to our study. First, as we mentioned, distinguishing state- versus trait-based contributions to individual differences in practice effects is difficult in the current study. Future studies should investigate the state vs. trait components of between-subjects variability in *H* by assessing it across multiple days of testing in both resting-state and task runs. Second, to assess whether practice effects indicated by *H* differences generalize to multiple cognitive tasks and evaluation schedules, other studies should examine a wider range of cognitive tasks and test-retest schedules to further extend our findings. Last but not least, as mentioned in the results, whole-brain *H* from the dual *n*-back task was trending as a sufficient predictor of performance change, and it is possible that with greater power, whole brain *H* would have led to successful classification of changes in performance in the DNB task. This was also the case for the word completion experiment, where whole-brain *H* was trending as being higher for the improvers compared to non-improvers ($t = 1.998$, $p = 0.052$). Indeed, when we tested the spatial specificity of the dual *n*-back ROI in word completion data, there was no difference in classification accuracy when using *H* from the whole brain compared to within the feature selected ROIs (i.e., classification was successful using whole-brain *H* of the first three runs of word completion, with mean accuracy = 67.9%, $p = 0.026$ compared to null distribution). This follows other research indicating classification in predictive models does not require the detail provided by precision mapping to be accurate because the features need not uniquely or specially facilitate prediction (Fair 2018, Nielsen et al., 2019). Thus, while our model is informative, it should not be conflated with precision mapping as the ROI spatial pattern is not unique. Furthermore, much of our research has pointed to differences in *H* across individuals and changes in *H* within individuals being a global (i.e., whole brain) and unidirectional effect (Churchill et al., 2016; Kardan et al., 2020; Stier et al., in preparation). Therefore, future studies can interrogate whether *H* predictors of changes in performance are indeed global, or vary specifically with different cognitive tasks.

In conclusion, the current study investigated the relationship between individual differences in practice-based improvements in cognitive task performance and respondents' level of scale-free BOLD activity. We found that individuals with higher fMRI *H* were more likely to improve their task performance when repeating the same cognitive task. In addition, to building upon previous work relating brain scale-invariance with overall behavioral performance, these results are the first to show how measures of scale invariance predict *changes* in behavioral

performance. These results provide empirical support for the hypothesis that brain networks impart functional advantages when their activity is in a more scale-free state. In addition to these theoretical contributions, our findings also have practical implications. Specifically, previous clinical research has proposed that variation in practice effects provide unique diagnostic and treatment information for clinical populations. For example, elder adults that show the expected practice effects in a test respond more to treatment for cognitive decline than those that do not show practice effects (Calero & Navarro, 2007; Duff, Beglinger, Moser, Schultz, & Paulsen, 2010; Fiszdon et al., 2006; Sergi, Kern, Mintz, & Green, 2005; Watzke, Brieger, Kuss, Schoettke, & Wiedl, 2008). However, the same line of research has found individual differences in practice effects for many cognitive tests to be uncorrelated with a wide range of demographic and cognitive ability scales that typically influence cognitive scores themselves (Duff et al, 2012; but also see Calamia, Markon, & Tranel, 2012). Our results suggest that *H* provides a promising avenue for future research in this field, as it appears capable of predicting who will improve with practice, irrespective of initial task performance at baseline. In summary, we find that individual variability in *H* across the brain may hold promise as a neural-marker of learning potential, which has wide-ranging theoretical and applied implications for cognitive neuroscience.

Methods

Participants

68 participants (41 female) aged between 18 and 40 years old (mean = 24.3 years, SD = 5.6 years) were recruited from the University of Chicago and surrounding area through fliers and geotargeted Facebook advertisements (30 White, 21 Asian, 13 Black, 4 Other). Twelve participants were excluded from analysis due to the following reasons: two participants were excluded due to incomplete fMRI data because of discomfort before the scanning session was finished; two were excluded due to technical issues with audio/visual during a run; five were flagged for sleepiness during the data acquisition as indicated by their eye-movement behavior by two on-site researchers (eye-movements were monitored using an MR-compatible EyeLink 1000 system); and five were excluded after the primary data quality check (see *fMRI data acquisition and preprocessing section*). Our final usable sample was N = 56.

All participants had self-reported normal or corrected-to-normal visual acuity and normal color vision. All participants provided written informed consent and were compensated $35 for

participation plus a potential bonus of $10. Participants were informed before the scanning session that if they "stayed attentive and still" during scans they would receive a $10 bonus. All participants who were not excluded based on the stated criteria above successfully received the bonus.

Experiment procedure

Participants arrived at the lab 45 minutes before the scanning session, and a research assistant provided detailed instructions for completing the audio-visual dual *n*-back (DNB) task. Each participant then performed a familiarization round of a dual 2-back and dual 3-back task (see the *Audio-visual dual n-back task section* for detail), with each round containing 22 and 23 trials, respectively. If the performance, measured with discrimination index A', was at or worse than chance level (i.e. $A' \leq 0.5$), additional rounds were completed until the participant declared they understood the task and performance exceeded chance.

After the in-lab task familiarization, participants walked to the hospital and the fMRI scanning session commenced. Following the collection of anatomical scans, 3 functional runs were acquired: a 7-min dual *n*-back run, a 10-min passive video watching run, and a second 7-min dual *n*-back run. Participants were randomly assigned to passively watch one of two videos during the video run: a video of non-nature tourist attractions in Europe or a video of outdoor nature scenes. Videos were roughly equated for aesthetic preference as rated by a different sample of 30 participants prior to this study (Likert scale1-7, $M_{nature} = 5.47$, SD = 1.14 and $M_{urban} = 4.77$, SD = 1.38), and did not include sound. After the scan session, participants were asked to give a preference rating (1-7 scale) for the video they watched. Ratings were included in subsequent analyses as a potential nuisance variable. At the beginning of each dual *n*-back run, participants were instructed to perform the task to the best of their ability.

fMRI data acquisition and preprocessing

Images were acquired on a Philips Achieva 3.0 T scanner with a standard quadrature 32-channel head coil at University of Chicago MRI Research Center. A T1-weighted gradient echo (MP-RAGE) was used to acquire high-resolution anatomical images for each participant (TR = 8 ms, TE = 3.5 ms, flip angle = 8°, FOV = 240 mm × 228 mm× 171 mm, matrix size = 240 × 228, in-plane resolution 1.0 mm^2, slice thickness = 1.0 mm, 171 sagittal slices). Functional T2* weighted images were acquired using an echo-planar sequence (TR = 2000 ms, TE = 26 ms, flip angle = 77°, FOV = 208 mm × 208 mm× 143.25 mm, matrix size = 64 × 64, in-plane resolution 3.25 mm^2, slice thickness

= 3.25 mm with 0.25 mm gap, 41 transverse-oblique slices parallel to the A-P line) during the dual *n*-back runs (241 volumes for each run) and the video run (305 volumes).

Initial data quality checks were performed using MRIQC (Esteban et al., 2017), which revealed excessive head movement and low tSNR (peak frame displacement > 2 mm, mean frame displacement > 0.2 mm, or tSNR < 50) for 5 participants during at least one of the scanning runs. These participants were excluded from analysis. The first 5 TRs of each functional run were discarded for all participants. Image preprocessing was completed using Advanced Normalization Tools (ANTs) (Avants, Tustison, & Song, 2009). The processing included bias correction for magnetic field inhomogeneity in both functional and anatomical data (*N4* algorithm in ANTs; (Tustison et al., 2010), affine motion correction of functional data using *antsMotionCorr* in ANTs, co-registering participants' anatomical data to their averaged functional data in each run using the symmetric normalization algorithm [*SyN*; (Avants et al., 2011)] in ANTs, warping anatomical images to the ICBM-152 template, and finally applying the combined transformation matrices of the two previous steps (coregistration and warping) to the functional data. Denoising included nuisance regression of 3 Principal Components of 24 motion parameters (6 translational and angular movements and their squares, derivatives, and squares of derivatives), linear and quadratic detrending, and band-pass filtering to [0.01, 0.1] Hz for removing physiological noise and drift.

Audio-visual dual n-back

In an *n*-back task, participants are instructed to press a button if the current visual or auditory stimulus matches the stimulus that was presented '*n*' previous trials back. The dual *n*-back (DNB) is a variant of this task in which two stimuli are presented simultaneously. Here, these stimuli were spoken integers, 1-9, and a blue square whose position varied in a 3 x 3 grid (see Figure 7). The paradigm was implemented in MATLAB and its code is publicly available at https://enl.uchicago.edu/stimuli-software/ (Layden, 2018).

On each trial of the dual n-back task, participants pressed their right index finger, right middle finger, both fingers, or neither finger, to indicate a position match, a number match, both a position and number match, or no match. Each trial lasted 3000 ms and the button press was permitted throughout the trial. Immediate feedback was provided to participants via red (incorrect press) or green (correct press) text at the bottom of the screen (see Figure 7).

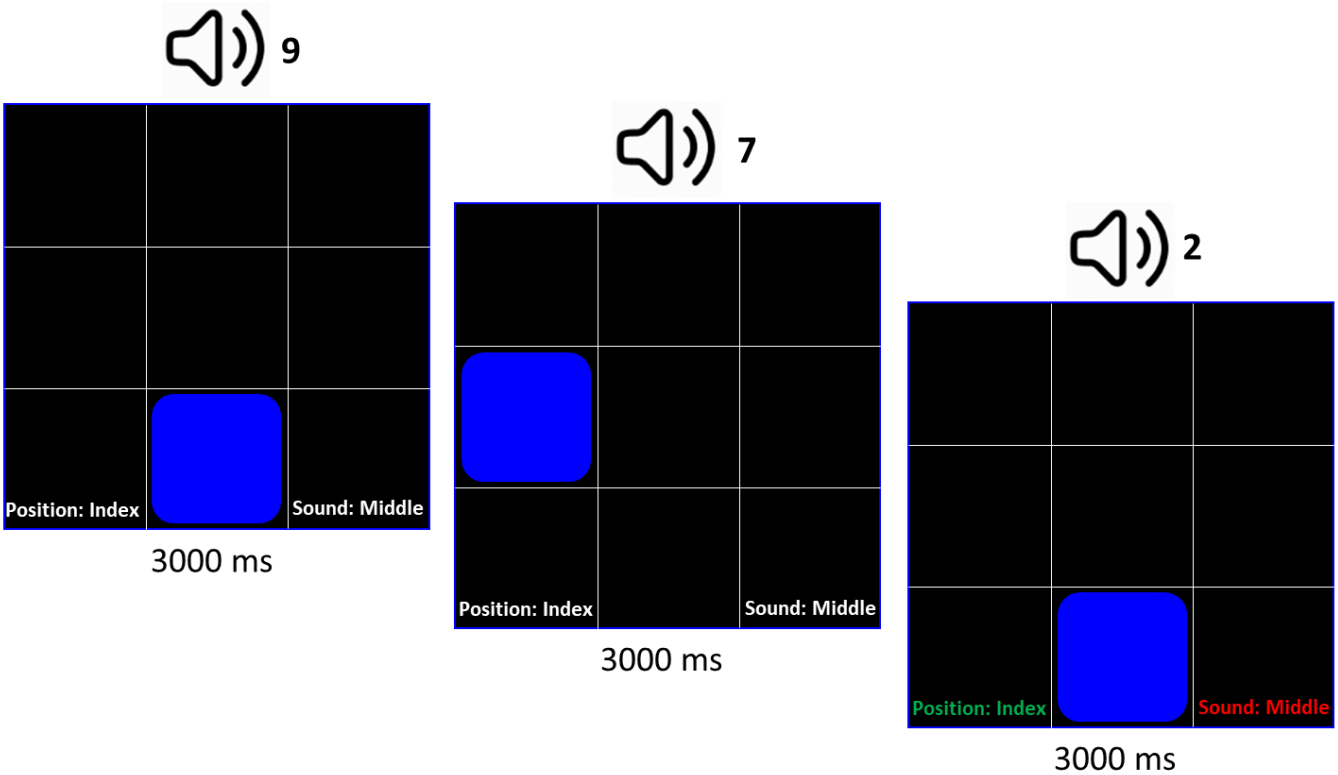

Figure 7. Audio-visual dual *n*-back task paradigm. In this example of the first three trials in a dual 2-back round, the participant correctly pressed their index finger for a match between the current and 2-back position of blue square, but falsely pressed their middle finger when they should not have (i.e., 2 does not match 9; so the correct response was only an index finger response and not an index finger and middle finger response). This is an example of 1 hit and 1 false alarm.

Performance improvers vs. non-improvers

Each functional MRI run included 6 blocks of the dual *n*-back task (four 2-back blocks and two 3-back blocks). Each block contained 20+*n* trials (*n* = 2 or 3), resulting in a total of 134 trials per dual *n*-back fMRI run. Blocks were separated by a 10-sec countdown that indicated whether the upcoming task would be 2-back or 3-back. As in the practice, the discrimination index A' (Stanislaw & Todorov, 1999) was used as the main performance measure. A' is similar to other sensitivity indices such as d', but is more robust to non-normality of responses (Stanislaw & Todorov, 1999). Furthermore, unlike d', A' = 0.5 corresponds to chance level performance, A' = 1 corresponds to perfect performance, and A'<0.5 corresponds to performance that is systematically worse than chance. A' is calculated as follows:

$$A' = 0.5 + sign(Hit - FA) * \frac{\left[(Hit - FA)^2 + abs(Hit - FA)\right]}{(4 * max(Hit, FA) - 4 * Hit * FA)}$$

Where *Hit* is the number of correct button presses and *FA* is the number of false alarms for both numbers and positions in a task block, where *sign(Hit - FA)* equals: +1 if (Hit - FA) > 0, 0 if (Hit - FA) = 0, and -1 if (Hit - FA) < 0, and where *max(Hit, FA)* equals the bigger value between Hit and FA.

Estimation of scale-free activity (H) and strength of functional connections (r^2)

Following our hypothesis, to evaluate the degree of scale-free dynamics of BOLD and its relationship to practice effects between individuals, we estimated the Hurst Exponent (H) of the fMRI timeseries from all 3 functional runs in for each participant (i.e., DNB-1, video watching and DNB-2). There are many different methods to estimate H. Here we used both detrended fluctuations analysis (DFA) and wavelet leader multifractal (WLMF) formalisms, both of which are robust to signal non-stationary and low-frequency confounds (Churchill et al., 2016; Jaffard, Lashermes, & Abry, 2007; Peng et al., 1995). The estimations were done on a voxel-wise level, and the DFA estimations of H were highly correlated with the first-order cumulant (i.e., mono-fractal) estimations of H from the WLMF. As such, further analysis was carried out using the DFA estimates, as this method is more computationally efficient.

To elaborate DFA, consider the linearly detrended BOLD timeseries $x(t)$ in a voxel over a run of total length$T$. This signal is first integrated and transformed into a cumulative sum $y(t)$, where $y(t) = \sum_{i=1}^{t}(x(i) - x_{ave})$; $t = 1, \dots, T$. $x(i)$ is the ith data point in the timeseries and x_{ave} is the average amplitude over all of the timeseries. Next, $y(t)$ is divided into windows of equal length n. A least-square linear regression is fit to each subdivision of $y(t)$ with length n, with the fitted values denoted as $\hat{y}_n(t)$. Next we detrend the integrated timeseries $y(t)$ by subtracting the local trend (i.e., the local least-squares straight-line fit), $\hat{y}_n(t)$ in each window. The root-mean-square magnitude of fluctuations on the detrended data $F(n)$ is then computed over a range of window sizes:

$$F(n) = \sqrt{\frac{1}{T}\sum_{t=1}^{T}[y(t) - \hat{y}_n(t)]^2}$$

Where n = 50 TRs is maximum window size corresponding to 0.01 Hz minimum frequency in the current study, and n = 3 TRs is minimum window size for fitting a line with a non-zero residual. Finally, the linear fit of $log(n)$ vs. $log(F(n))$ is calculated and the slope of this fitted line is used as the estimate of the degree of scale-invariance (H) for the voxel time-series $x(t)$. A slope of H = 0.5

indicates no long-range correlation in the signal (i.e., a random walk), while *H* values closer to 1 indicate greater scale-invariance.

We also quantified the strength of statistical dependency between brain regions (i.e., magnitude of functional connections) in the three functional runs to be used as a control variable when assessing *H* based classification model. The data was first down-sampled to 392 regions by averaging voxel-level time-series within each region of the CC-400 brain atlas (Craddock, James, Holtzheimer, Hu, & Mayberg, 2012), and the Pearson correlation between every pair of regions was calculated and squared (r^2). The squared r was used to be agnostic towards the sign of correlation when averaging over connectivity strengths in the classification step to keep everything consistent between *H* and functional connectivity models. However, a supplementary analysis where Fisher z-transformed correlations with negative and positive signs were averaged separately showed no difference in classification results using functional connectivity.[3] The down-sampling was done to reduce the number of pairwise connections (76,636 vs. ~2 billion pairs from the non-down sampled voxel space data). The CC-400 atlas was used because it provided 76K pairwise connections, which is a similar order of magnitude to the number of voxels for the *H*-based analysis, thus keeping the *H* and r^2 matrices used for defining regions and functional connections of interest for classifications comparable in size.

Classification of improvers vs. non-improvers using ROI and COI average H or r^2

The *H* and r^2 in fMRI functional runs 1 and 2 (dual *n*-back 1 and video) were averaged over the selected ROI and COI for each participant and were each used to classify the improvers and non-improvers in a linear discriminant (LD) classification implemented in MATLAB (R2016b, The MathWorks, Inc., Natick, Massachusetts, United States) with leave-one-participant-out cross-validation. Please note that since there is only one feature used in the classification (a subject has one averaged value of *H* or r^2), the procedure is to simply compare the left-out subject's *H* or r^2 value with the mean of *H* or r^2 values in the training data. The left-out subject is then classified as improver or non-improver based on whether their *H* or r^2 is closer to the mean of non-left-out improvers or non-improvers. A distribution of classification accuracies was constructed by bootstrapping (1000 resamples with replacement) the participants with intact class labels (improver vs. non-improver). Predictive power of each feature (i. e., H_{DNB1}, H_{Vid}, $Conn_{DNB1}$, or

[3] In fact a Support Vector Machine classification trained with all of the functional connections in run 3 (i.e., no averaging over connections) still performed worse than chance when classifying improvers from non-improvers in the test datasets run1 and run2.

$Conn_{Vid}$) was then tested against a null distribution with permuted class labels to test for statistical significance of classifications.

Independent sample replication of results relating average H to practice effects

We also used the average *H* over the same ROIs from the dual *n*-back experiment dataset to predict improvers and non-improvers in an independent sample of 45 subjects performing a completely different working memory and attention task (a word completion task). The dataset was provided by Choe, Jenifer, Rozek, Berman, & Beilock (in preparation), and consists of fMRI runs for 45 participants aged between 18-35 who performed a math and word Choose-and-Solve Task (CAST) for 6 minutes in every run. This task involves choosing to solve math equation completion and word completion tasks and is originally designed for detecting math anxiety and math avoidance behavior (Choe et al., 2019). The participants performed the CAST in 6 runs in fMRI scanner which provided us with a different learning/practice paradigm to cross-validate the *H*-based classification model used for dual *n*-back. The questions were designated as having a 1-7 difficulty level (Choe et al., 2019). The performance of participants in CAST was quantified as their accuracy*difficulty level of questions they solved, since the question difficulty was adaptive in a manner that two correct answers in a row would result in an increase in difficulty and one wrong answer would result in decrease in question difficulty. Since the number of trials where difficult math questions (with higher reward) were chosen over easy math questions (with lower reward) was very sparse across participants, performance was quantified only over word-completion trials.

In word completion trials, participants see words with omitted letters replaced by ~ and □. The participant has to quickly choose (< 2000 msec) the correct letter that should be in the square (i. e., □). For example, for E~□DE~CE, the correct choice is letter 'I' (the word is 'evidence'). In this dataset, the fMRI acquisition parameters were identical to our dual *n*-back dataset and we pre-processed and calculated *H* values identically to the dual *n*-back dataset. The improvers and non-improvers were labeled by a median split on change in performance between last run compared to first run, adjusted for performance in the first run, similar to the dual *n*-back dataset. The improvers had an average increase of 23% on their task performance compared to a decrease of -16% for non-improvers.

Acknowledgments

This work was supported in part by a grant from the TKF Foundation to M.G.B. a grant from the

National Science Foundation (BCS-1632445) to M.G.B., a Grossman Institute for Neuroscience, Quantitative Biology, and Human Behavior from the University of Chicago [Pilot MRI Award to M.G.B. and S.L.B.; Sahred Equipment Award to M.G.B.], and an internal grant from University of Chicago to M.G.B.

References

Adam, K. C. S., Robison, M. K., & Vogel, E. K. (2018). Contralateral Delay Activity Tracks Fluctuations in Working Memory Performance. *Journal of Cognitive Neuroscience*, *30*(9), 1229–1240. https://doi.org/10.1162/jocn_a_01233

Arviv, O., Goldstein, A., & Shriki, O. (2015). Near-Critical Dynamics in Stimulus-Evoked Activity of the Human Brain and Its Relation to Spontaneous Resting-State Activity. *Journal of Neuroscience*, *35*(41), 13927–13942. https://doi.org/10.1523/JNEUROSCI.0477-15.2015

Avants, B. B., Tustison, N. J., Song, G., Cook, P. A., Klein, A., & Gee, J. C. (2011). A reproducible evaluation of ANTs similarity metric performance in brain image registration. *Neuroimage*, *54*(3), 2033–2044.

Avants, B. B., Tustison, N., & Song, G. (2009). Advanced normalization tools (ANTS). *Insight j*, *2*, 1–35.

Awh, E., & Jonides, J. (2001). Overlapping mechanisms of attention and spatial working memory. *Trends in Cognitive Sciences*, *5*(3), 119–126. https://doi.org/10.1016/S1364-6613(00)01593-X

Bassett, D. S., Meyer-Lindenberg, A., Achard, S., Duke, T., & Bullmore, E. (2006). Adaptive reconfiguration of fractal small-world human brain functional networks. *Proceedings of the National Academy of Sciences*, *103*(51), 19518–19523. https://doi.org/10.1073/pnas.0606005103

Beggs, J. M. (2008). The criticality hypothesis: how local cortical networks might optimize information processing. *Philosophical Transactions of the Royal Society A: Mathematical, Physical and Engineering Sciences*, *366*(1864), 329-343.

Biazoli, C. E. J., Salum, G. A., Pan, P. M., Zugman, A., Amaro, E. J., Rohde, L. A., … Sato, J. R. (2017). Commentary: Functional connectome fingerprint: identifying individuals using patterns of brain connectivity. *Frontiers in Human Neuroscience*, *11*. https://doi.org/10.3389/fnhum.2017.00047

Boedecker, J., Obst, O., Lizier, J. T., Mayer, N. M., & Asada, M. (2012). Information processing in echo state networks at the edge of chaos. *Theory in Biosciences*, *131*(3), 205–213. https://doi.org/10.1007/s12064-011-0146-8

Calamia, M., Markon, K., & Tranel, D. (2012). Scoring higher the second time around: meta-analyses of practice effects in neuropsychological assessment. *The Clinical Neuropsychologist*, *26*(4), 543-570.

Chialvo, D. R. (2004). Critical brain networks. *Physica A: Statistical Mechanics and Its Applications*, *340*(4), 756–765. https://doi.org/10.1016/j.physa.2004.05.064

Chialvo, D. R. (2010). Emergent complex neural dynamics. *Nature Physics*, *6*(10), 744–750. https://doi.org/10.1038/nphys1803

Choe, K. W., Jenifer, J. B., Rozek, C. S., Berman, M. G., & Beilock, S. L. (2019). Calculated avoidance: Math anxiety predicts math avoidance in effort-based decision-making. *Science advances*, *5*(11), eaay1062.

Churchill, N. W., Cimprich, B., Askren, M. K., Reuter-Lorenz, P. A., Jung, M. S., Peltier, S., & Berman, M. G. (2015). Scale-free brain dynamics under physical and psychological distress: Pre-treatment effects in women diagnosed with breast cancer. *Human Brain Mapping*, *36*(3), 1077–1092. https://doi.org/10.1002/hbm.22687

Churchill, N. W., Spring, R., Grady, C., Cimprich, B., Askren, M. K., Reuter-Lorenz, P. A., … Berman, M. G. (2016). The suppression of scale-free fMRI brain dynamics across three different sources of effort: Aging, task novelty and task difficulty. *Scientific Reports*, *6*, 30895. https://doi.org/10.1038/srep30895

Churchill, N. W., Hutchison, M. G., Graham, S. J., & Schweizer, T. A. (2020). Scale-free functional brain dynamics during recovery from sport-related concussion. *Human brain mapping*.

Ciuciu, P., Abry, P., & He, B. J. (2014). Interplay between functional connectivity and scale-free dynamics in intrinsic fMRI networks. *NeuroImage*, *95*, 248–263. https://doi.org/10.1016/j.neuroimage.2014.03.047

Cocchi, L., Gollo, L. L., Zalesky, A., & Breakspear, M. (2017). Criticality in the brain: A synthesis of neurobiology, models and cognition. *Progress in Neurobiology*, *158*, 132–152. https://doi.org/10.1016/j.pneurobio.2017.07.002

Craddock, R. C., James, G. A., Holtzheimer, P. E., Hu, X. P., & Mayberg, H. S. (2012). A whole brain fMRI atlas generated via spatially constrained spectral clustering. *Human Brain Mapping*, *33*(8), 1914–1928. https://doi.org/10.1002/hbm.21333

de Arcangelis, L., & Herrmann, H. J. (2010). Learning as a phenomenon occurring in a critical state. *Proceedings of the National Academy of Sciences*, *107*(9), 3977–3981. https://doi.org/10.1073/pnas.0912289107

de Arcangelis, L., Perrone-Capano, C., & Herrmann, H. J. (2006). Self-Organized Criticality Model for Brain Plasticity. *Physical Review Letters*, *96*(2), 028107. https://doi.org/10.1103/PhysRevLett.96.028107

Duff, K., Callister, C., Dennett, K., & Tometich, D. (2012). Practice effects: a unique cognitive variable. *The Clinical Neuropsychologist*, *26*(7), 1117-1127.

Esteban, O., Birman, D., Schaer, M., Koyejo, O. O., Poldrack, R. A., & Gorgolewski, K. J. (2017). MRIQC: Advancing the automatic prediction of image quality in MRI from unseen sites. *PLOS ONE*, *12*(9), e0184661. https://doi.org/10.1371/journal.pone.0184661

Fagerholm, E. D., Lorenz, R., Scott, G., Dinov, M., Hellyer, P. J., Mirzaei, N., … Leech, R. (2015). Cascades and Cognitive State: Focused Attention Incurs Subcritical Dynamics. *Journal of Neuroscience*, *35*(11), 4626–4634. https://doi.org/10.1523/JNEUROSCI.3694-14.2015

Fair, D. A. (2018). The Big Reveal: Precision Mapping Shines a Gigantic Floodlight on the Cerebellum. *Neuron*, *100*(4), 773-776.

Fraiman, D., Balenzuela, P., Foss, J., & Chialvo, D. R. (2009). Ising-like dynamics in large-scale functional brain networks. *Physical Review E*, *79*(6), 061922. https://doi.org/10.1103/PhysRevE.79.061922

Frette, V., Christensen, K., Malthe-Sørenssen, A., Feder, J., Jøssang, T., & Meakin, P. (1996). Avalanche dynamics in a pile of rice. *Nature*, *379*(6560), 49. https://doi.org/10.1038/379049a0

Gautam, S. H., Hoang, T. T., McClanahan, K., Grady, S. K., & Shew, W. L. (2015). Maximizing Sensory Dynamic Range by Tuning the Cortical State to Criticality. *PLOS Computational Biology*, *11*(12), e1004576. https://doi.org/10.1371/journal.pcbi.1004576

Gisiger, T. (2001). Scale invariance in biology: Coincidence or footprint of a universal mechanism? *Biological Reviews*, *76*(2), 161–209. https://doi.org/10.1017/S1464793101005607

Goldberger, A. L., Amaral, L. A. N., Hausdorff, J. M., Ivanov, P. C., Peng, C.-K., & Stanley, H. E. (2002). Fractal dynamics in physiology: Alterations with disease and aging. *Proceedings of the National Academy of Sciences*, *99*(suppl 1), 2466–2472. https://doi.org/10.1073/pnas.012579499

Gollo, L. L. (2017). Coexistence of critical sensitivity and subcritical specificity can yield optimal population coding. *Journal of The Royal Society Interface*, *14*(134), 20170207. https://doi.org/10.1098/rsif.2017.0207

Gonzalez-Castillo, J., & Bandettini, P. A. (2018). Task-based dynamic functional connectivity: Recent findings and open questions. *NeuroImage*, *180*, 526–533. https://doi.org/10.1016/j.neuroimage.2017.08.006

Hahn, G., Ponce-Alvarez, A., Monier, C., Benvenuti, G., Kumar, A., Chavane, F., … Frégnac, Y. (2017). Spontaneous cortical activity is transiently poised close to criticality. *PLOS Computational Biology*, *13*(5), e1005543. https://doi.org/10.1371/journal.pcbi.1005543

He, B. J. (2011). Scale-Free Properties of the Functional Magnetic Resonance Imaging Signal during Rest and Task. *Journal of Neuroscience*, *31*(39), 13786–13795. https://doi.org/10.1523/JNEUROSCI.2111-11.2011

He, B. J. (2014). Scale-free brain activity: Past, present, and future. *Trends in Cognitive Sciences*, *18*(9), 480–487. https://doi.org/10.1016/j.tics.2014.04.003

Hutchison, R. M., Womelsdorf, T., Allen, E. A., Bandettini, P. A., Calhoun, V. D., Corbetta, M., … Chang, C. (2013). Dynamic functional connectivity: Promise, issues, and interpretations. *NeuroImage*, *80*. https://doi.org/10.1016/j.neuroimage.2013.05.079

Ikkai, A., & Curtis, C. E. (2011). Common neural mechanisms supporting spatial working memory, attention and motor intention. *Neuropsychologia*, *49*(6), 1428–1434. https://doi.org/10.1016/j.neuropsychologia.2010.12.020

Jaeggi, S. M., Buschkuehl, M., Jonides, J., & Perrig, W. J. (2008). Improving fluid intelligence with training on working memory. *Proceedings of the National Academy of Sciences*, *105*(19), 6829. https://doi.org/10.1073/pnas.0801268105

Kardan, O., Adam, K. C., Mance, I., Churchill, N. W., Vogel, E. K., & Berman, M. G. (2020). Distinguishing cognitive effort and working memory load using scale-invariance and alpha suppression in EEG. *NeuroImage*, *211*, 116622.

Kardan, O., Berman, M. G., Yourganov, G., Schmidt, J., & Henderson, J. M. (2015). Classifying mental states from eye movements during scene viewing. *Journal of Experimental Psychology. Human Perception and Performance*, *41*(6), 1502–1514. https://doi.org/10.1037/a0039673

Kardan, O., Henderson, J. M., Yourganov, G., & Berman, M. G. (2016). Observers' cognitive states modulate how visual inputs relate to gaze control. *Journal of Experimental Psychology. Human Perception and Performance*, *42*(9), 1429–1442. https://doi.org/10.1037/xhp0000224

Kardan, O., Reuter-Lorenz, P. A., Peltier, S., Churchill, N. W., Misic, B., Askren, M. K., … Berman, M. G. (2019). Brain connectivity tracks effects of chemotherapy separately from behavioral measures. *NeuroImage: Clinical*, 101654. https://doi.org/10.1016/j.nicl.2019.101654

Kinouchi, O., & Copelli, M. (2006). Optimal dynamical range of excitable networks at criticality. *Nature Physics*, *2*(5), 348. https://doi.org/10.1038/nphys289

Kirk, R. E. (2012). Experimental Design. In *Handbook of Psychology, Second Edition*. https://doi.org/10.1002/9781118133880.hop202001

Kitzbichler, M. G., Smith, M. L., Christensen, S. R., & Bullmore, E. (2009). Broadband Criticality of Human Brain Network Synchronization. *PLOS Computational Biology*, *5*(3), e1000314. https://doi.org/10.1371/journal.pcbi.1000314

Latham, P. E., & Nirenberg, S. (2004). Computing and Stability in Cortical Networks. *Neural Computation*, *16*(7), 1385–1412. https://doi.org/10.1162/089976604323057434

Layden, E. A. (2018). *N-Back for Matlab*. Retrieved from https://doi.org/10.12751/g-node.f87128

Muñoz, M. A. (2018). Colloquium: Criticality and dynamical scaling in living systems. *Reviews of Modern Physics*, *90*(3), 031001. https://doi.org/10.1103/RevModPhys.90.031001

Neubauer, A. C., & Fink, A. (2009). Intelligence and neural efficiency. *Neuroscience & Biobehavioral Reviews*, *33*(7), 1004-1023.

Neubauer, A. C., & Fink, A. (2009). Intelligence and neural efficiency: Measures of brain activation versus measures of functional connectivity in the brain. *Intelligence*, *37*(2), 223-229.

Nielsen, A. N., Greene, D. J., Gratton, C., Dosenbach, N. U., Petersen, S. E., & Schlaggar, B. L. (2019). Evaluating the prediction of brain maturity from functional connectivity after motion artifact denoising. *Cerebral Cortex*, *29*(6), 2455-2469.

Peng, C. K., Havlin, S., Hausdorff, J. M., Mietus, J. E., Stanley, H. E., & Goldberger, A. L. (1995). Fractal mechanisms and heart rate dynamics: long-range correlations and their breakdown with disease. *Journal of electrocardiology*, *28*, 59-65.

Proekt, A., Banavar, J. R., Maritan, A., & Pfaff, D. W. (2012). Scale invariance in the dynamics of spontaneous behavior. *Proceedings of the National Academy of Sciences*, *109*(26), 10564–10569. https://doi.org/10.1073/pnas.1206894109

Rapport, L. J., Brines, D. B., Theisen, M. E., & Axelrod, B. N. (1997). Full scale IQ as mediator of practice effects: The rich get richer. *The Clinical Neuropsychologist*, *11*(4), 375-380.

Rosenberg, M. D., Finn, E. S., Scheinost, D., Papademetris, X., Shen, X., Constable, R. T., & Chun, M. M. (2016). A neuromarker of sustained attention from whole-brain functional connectivity. *Nature Neuroscience*, *19*(1), 165–171. https://doi.org/10.1038/nn.4179

Rosenberg, M. D., Scheinost, D., Greene, A. S., Avery, E. W., Kwon, Y. H., Finn, E. S., ... & Chun, M. M. (2020). Functional connectivity predicts changes in attention observed across minutes, days, and months. *Proceedings of the National Academy of Sciences*, *117*(7), 3797-3807.

Shen, X., Finn, E. S., Scheinost, D., Rosenberg, M. D., Chun, M. M., Papademetris, X., & Constable, R. T. (2017). Using connectome-based predictive modeling to predict individual behavior from brain connectivity. *Nature Protocols*, *12*(3), 506–518. https://doi.org/10.1038/nprot.2016.178

Shew, W. L., & Plenz, D. (2013). The Functional Benefits of Criticality in the Cortex. *The Neuroscientist*, *19*(1), 88–100. https://doi.org/10.1177/1073858412445487

Shine, J. M., Koyejo, O., & Poldrack, R. A. (2016). Temporal metastates are associated with differential patterns of time-resolved connectivity, network topology, and attention. *Proceedings of the National Academy of Sciences*, *113*(35), 9888–9891. https://doi.org/10.1073/pnas.1604898113

Shirer, W. R., Ryali, S., Rykhlevskaia, E., Menon, V., & Greicius, M. D. (2012). Decoding Subject-Driven Cognitive States with Whole-Brain Connectivity Patterns. *Cerebral Cortex*, *22*(1), 158–165. https://doi.org/10.1093/cercor/bhr099

Shriki, O., Alstott, J., Carver, F., Holroyd, T., Henson, R. N. A., Smith, M. L., … Plenz, D. (2013). Neuronal Avalanches in the Resting MEG of the Human Brain. *Journal of Neuroscience*, *33*(16), 7079–7090. https://doi.org/10.1523/JNEUROSCI.4286-12.2013

Shriki, O., & Yellin, D. (2016). Optimal Information Representation and Criticality in an Adaptive Sensory Recurrent Neuronal Network. *PLOS Computational Biology*, *12*(2), e1004698. https://doi.org/10.1371/journal.pcbi.1004698

Smith, S. M., Nichols, T. E., Vidaurre, D., Winkler, A. M., Behrens, T. E. J., Glasser, M. F., … Miller, K. L. (2015). A positive-negative mode of population covariation links brain connectivity,

demographics and behavior. *Nature Neuroscience*, *18*(11), 1565–1567. https://doi.org/10.1038/nn.4125

Stanislaw, H., & Todorov, N. (1999). Calculation of signal detection theory measures. *Behavior Research Methods, Instruments, & Computers*, *31*(1), 137–149. https://doi.org/10.3758/BF03207704

Tanaka, T., Kaneko, T., & Aoyagi, T. (2008). Recurrent Infomax Generates Cell Assemblies, Neuronal Avalanches, and Simple Cell-Like Selectivity. *Neural Computation*, *21*(4), 1038–1067. https://doi.org/10.1162/neco.2008.03-08-727

Tustison, N. J., Avants, B. B., Cook, P. A., Zheng, Y., Egan, A., Yushkevich, P. A., & Gee, J. C. (2010). N4ITK: Improved N3 bias correction. *IEEE Transactions on Medical Imaging*, *29*(6), 1310–1320.

von Wegner, F., Laufs, H., & Tagliazucchi, E. (2018). Mutual information identifies spurious Hurst phenomena in resting state EEG and fMRI data. *Physical Review E*, *97*(2). https://doi.org/10.1103/PhysRevE.97.022415

Werner, G. (2010). Fractals in the nervous system: Conceptual implications for theoretical neuroscience. *Frontiers in Physiology*, *1*. https://doi.org/10.3389/fphys.2010.00015

Yamashita, M., Yoshihara, Y., Hashimoto, R., Yahata, N., Ichikawa, N., Sakai, Y., … Imamizu, H. (2018). A prediction model of working memory across health and psychiatric disease using whole-brain functional connectivity. *Elife*, *7*. Retrieved from http://publications.eng.cam.ac.uk/1042306/

Yu, S., Ribeiro, T. L., Meisel, C., Chou, S., Mitz, A., Saunders, R., & Plenz, D. (2017). Maintained avalanche dynamics during task-induced changes of neuronal activity in nonhuman primates. *ELife*, *6*, e27119. https://doi.org/10.7554/eLife.27119

Supplementary Material

Figure S1. Classification accuracy distributions and confusion matrices when the classes are based on median split of ΔA' non-adjusted for baseline performance in panel **A**, with corresponding confusion matrices shown in panel **B**. In panel A, each box-plot shows all the distribution of accuracies using the model indicated on the x-axis. The p values compare the null model distribution with models containing the variable indicated on the *x*-axis. M shows mean of the distribution of accuracies (so do black horizontal ticks inside the boxes), notch in the boxes show medians of distributions, and thick teal vertical lines show the SD of distributions around the means. The boxes show ±1 quantile around the median and whiskers show range of the distribution. All statistics reported included all 1,000 bootstrap sample accuracies. In panel B, rows show true labels of the classes of improvers (labeled high) and non-improvers (labeled low), and columns show predicted labels. In confusion matrices higher values in main diagonals indicate better classification, while higher values off main diagonals indicates proportion of misclassified individuals. Note: When using non-adjusted ΔA', the defined non-improver group had a significantly higher baseline performance (A'_0 = 0.850 for non-improvers and 0.803 for improvers, t = 2.244, p = 0.029), but the improvers performed equally well, if not better, the second time around resulting in a non-significant difference in secondary performance (A'_f = 0.860 for non-improvers and 0.883 for improvers, t =1.102, p = 0.275).

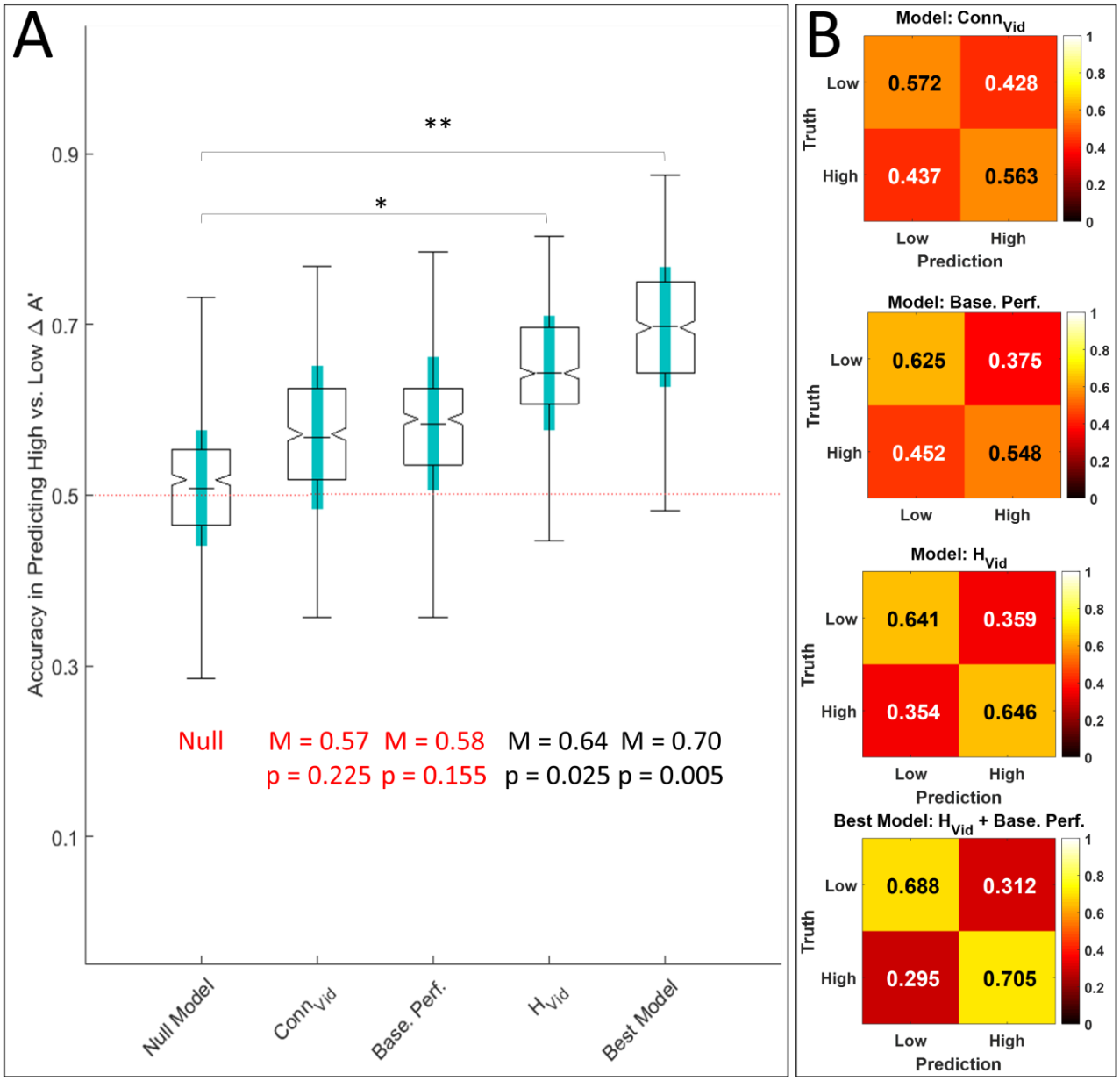
A
Accuracy in Predicting High vs. Low Δ A'
0.9
0.7
0.5
0.3
0.1
**
*
Null
M = 0.57
p = 0.225
M = 0.58
p = 0.155
M = 0.64
p = 0.025
M = 0.70
p = 0.005
Null Model
Conn Vid
Base. Perf.
H Vid
Best Model
B
Model: Conn Vid
Low
High
Truth
0.572
0.428
0.437
0.563
Low
High
Prediction
Model: Base. Perf.
0.625
0.375
0.452
0.548
Model: H Vid
0.641
0.359
0.354
0.646
Best Model: H Vid + Base. Perf.
0.688
0.312
0.295
0.705
1
0.8
0.6
0.4
0.2
0

Figure S2. Steps in selection of voxels (ROI) and pairwise functional connections (COI) that enhance the distinction in H and functional connectivity between task improvers and non-improvers based on run 3 of the fMRI session in dual *n*-back task. The *H* and r^2 from prior runs (DNB1 and Video) are then averaged in these selected ROI and COI for each participant, denoted as H_{Vid} or H_{DNB1} and $Conn_{Vid}$ or $Conn_{DNB1}$ respectively, and used for classification in the DNB data. The same ROI and COI are also later used in the independent fMRI dataset of word completion task.

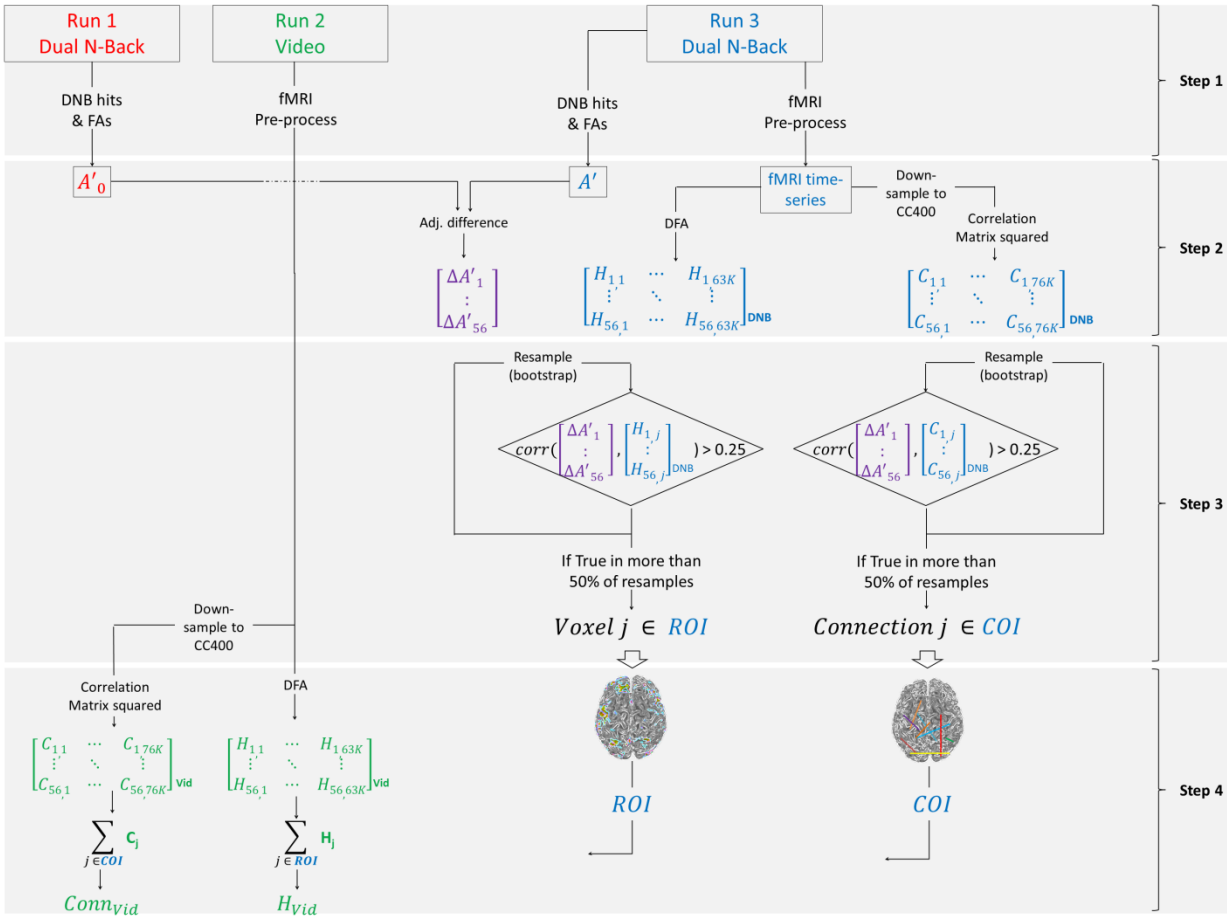

Table S1. The % of the ROI voxels used for classification in each anatomically significant brain structure is listed below. The structures with less than 10 voxels overlap (i. e., < 0.2% overlap) are omitted for brevity.

Brain Structure	% Overlap of ROI
White Matter	57.54
Left Cerebrum	46.80
Right Cerebrum	41.46
Frontal Lobe	36.02
Gray Matter	25.43
Temporal Lobe	17.63
Sub-Gyral	17.11
Sub-lobar	15.25
Middle Frontal Gyrus	8.90
Extra-Nuclear	7.08
Limbic Lobe	6.99
Parietal Lobe	6.46
Precentral Gyrus	6.03
Inferior Frontal Gyrus	5.95
Occipital Lobe	5.77
Superior Temporal Gyrus	5.69
Left Cerebellum	5.65
Middle Temporal Gyrus	5.13
Precentral_R (aal)	4.53
Cerebellum Posterior Lobe	4.26
Frontal_Mid_L (aal)	4.13
Cingulate Gyrus	4.04
Superior Frontal Gyrus	4.00
Thalamus	3.51
brodmann area 6	3.46
Temporal_Mid_L (aal)	3.40
Middle Occipital Gyrus	2.80
Postcentral Gyrus	2.78
Cerebellar Tonsil	2.63
Thalamus_R (aal)	2.54
Temporal_Sup_R (aal)	2.42
Insula	2.33
Frontal_Mid_R (aal)	2.29
Precentral_L (aal)	2.29
Frontal_Sup_L (aal)	2.08
Frontal_Inf_Oper_R (aal)	2.01

Postcentral_L (aal)	1.97
Frontal_Inf_Tri_L (aal)	1.95
Cingulum_Mid_R (aal)	1.93
Temporal_Sup_L (aal)	1.77
Frontal_Inf_Tri_R (aal)	1.75
Occipital_Mid_L (aal)	1.71
brodmann area 9	1.69
Medial Frontal Gyrus	1.69
Corpus Callosum	1.65
Occipital_Mid_R (aal)	1.63
brodmann area 10	1.62
brodmann area 22	1.54
Cerebro-Spinal Fluid	1.54
Temporal_Inf_L (aal)	1.52
Lateral Ventricle	1.52
Pulvinar	1.52
Parahippocampa Gyrus	1.48
Postcentral_R (aal)	1.45
Cerebellum Anterior Lobe	1.39
brodmann area 19	1.39
Inferior Parietal Lobule	1.35
Fusiform_L (aal)	1.31
Anterior Cingulate	1.22
Cerebelum_Crus1_L (aal)	1.18
Rolandic_Oper_R (aal)	1.15
Cerebelum_Crus2_L (aal)	1.13
Thalamus_L (aal)	1.11
brodmann area 8	1.03
Occipital_Inf_R (aal)	1.01
Culmen	1.00
Frontal_Sup_Medial_L (aal)	1.00
Parietal_Inf_L (aal)	0.98
Fusiform Gyrus	0.88
Cerebelum_8_L (aal)	0.88
Insula_L (aal)	0.85
brodmann area 21	0.83
brodmann area 13	0.83
Temporal_Mid_R (aal)	0.77
Caudate_L (aal)	0.75
Caudate	0.71
brodmann area 4	0.71

Frontal_Inf_Orb_L (aal)	0.69
Rolandic_Oper_L (aal)	0.69
Cingulum_Ant_R (aal)	0.69
Frontal_Mid_Orb_L (aal)	0.66
brodmann area 40	0.64
Paracentral Lobule	0.62
Inferior Semi-Lunar Lobule	0.62
SupraMarginal_L (aal)	0.62
Inferior Temporal Gyrus	0.60
Inter-Hemispheric	0.58
Lingual_L (aal)	0.58
Precuneus	0.58
Tuber	0.58
Precuneus_R (aal)	0.56
Cerebelum_9_L (aal)	0.54
brodmann area 31	0.54
brodmann area 37	0.54
brodmann area 3	0.53
brodmann area 39	0.53
Hippocampus_R (aal)	0.51
Insula_R (aal)	0.51
Cingulum_Mid_L (aal)	0.51
Caudate Body	0.51
Supp_Motor_Area_R (aal)	0.51
brodmann area 2	0.51
brodmann area 44	0.49
Inferior Occipital Gyrus	0.47
brodmann area 46	0.47
Frontal_Sup_Medial_R (aal)	0.47
Cerebelum_7b_L (aal)	0.43
Frontal_Sup_R (aal)	0.41
Hippocampus_L (aal)	0.39
Medial Dorsal Nucleus	0.39
Ventral Lateral Nucleus	0.39
brodmann area 18	0.39
brodmann area 24	0.38
Occipital_Sup_L (aal)	0.36
Precuneus_L (aal)	0.36
ParaHippocampal_L (aal)	0.36
Temporal_Inf_R (aal)	0.34
Cuneus	0.32

Temporal_Pole_Sup_L (aal)	0.32
brodmann area 32	0.32
brodmann area 41	0.32
Frontal_Inf_Oper_L (aal)	0.32
Midbrain	0.30
Calcarine_L (aal)	0.30
Right Brainstem	0.30
Supramarginal Gyrus	0.30
brodmann area 45	0.28
Cerebelum_6_L (aal)	0.28
brodmann area 20	0.28
Pyramis	0.26
Paracentral_Lobule_R (aal)	0.24
brodmann area 42	0.24
ParaHippocampal_R (aal)	0.24
Transverse Temporal Gyrus	0.23
brodmann area 47	0.23
Cingulum_Post_R (aal)	0.21
Caudate Tail	0.21
brodmann area 11	0.21
SupraMarginal_R (aal)	0.21
Putamen	0.19
Lentiform Nucleus	0.19

Table S2. The % connections in the classification COI for each node (CC-400 region), together with the AAL-116 (Automated Anatomical Labeling) anatomical labels of voxels in the node are shown below. Numbers in brackets in the AAL label column shows proportion of overlap between the AAL-116 region and the CC-400 region.

CC-400 region	% of COI	AAL label
1	0.4602	["Cerebelum_4_5_L": 0.64]["Lingual_L": 0.29]
2	0.5487	["Frontal_Sup_R": 0.51]["Frontal_Mid_R": 0.49]
3	0.1770	["Postcentral_L": 0.94]
4	0.4956	["Caudate_R": 0.96]
5	0.1062	["Temporal_Sup_R": 0.85]["SupraMarginal_R": 0.15]
6	0.0354	["Occipital_Mid_L": 0.77]["Temporal_Mid_L": 0.21]
7	0.2832	["Frontal_Mid_L": 0.63]["Frontal_Sup_L": 0.37]
8	0.1947	["Angular_R": 0.86]
9	0.8496	["Insula_L": 0.74]["Frontal_Inf_Tri_L": 0.19]

10	0.1239	["Rolandic_Oper_L": 0.39]["Heschl_L": 0.25]["Temporal_Sup_L": 0.25]["Insula_L": 0.12]
11	0.0354	["Precuneus_L": 0.36]["Precuneus_R": 0.32]["Cingulum_Post_L": 0.18]
12	0.0000	["Amygdala_R": 0.38]["Hippocampus_R": 0.36]["ParaHippocampal_R": 0.22]
13	0.3717	["Cerebelum_Crus1_L": 0.88]
14	0.5310	["Caudate_L": 0.98]
15	0.6372	["Frontal_Mid_R": 0.75]["Frontal_Inf_Oper_R": 0.25]
16	0.2655	["Frontal_Mid_R": 0.80]["Precentral_R": 0.13]
17	0.0177	["Cerebelum_Crus1_R": 0.89]["Cerebelum_Crus2_R": 0.11]
18	0.6549	["Cerebelum_6_L": 0.60]["Cerebelum_Crus1_L": 0.40]
19	0.1770	["Temporal_Pole_Sup_L": 0.80]["Temporal_Pole_Mid_L": 0.20]
20	0.4248	["Cingulum_Mid_L": 0.79]["Supp_Motor_Area_L": 0.21]
21	0.0708	["Thalamus_L": 0.91]
22	0.2124	["Rolandic_Oper_R": 0.55]["Insula_R": 0.40]
23	0.0885	["Postcentral_R": 0.85]["Precentral_R": 0.15]
24	0.0885	["Lingual_L": 0.43]["Cerebelum_Crus1_L": 0.28]["Calcarine_L": 0.14]
25	0.0000	["Frontal_Inf_Orb_L": 0.59]["Frontal_Mid_Orb_L": 0.38]
26	0.0354	["Temporal_Mid_R": 0.74]["Angular_R": 0.14]["Occipital_Mid_R": 0.12]
27	0.6018	["Vermis_4_5": 0.26]["Vermis_6": 0.16]["Vermis_10": 0.14]["Cerebelum_4_5_L": 0.12]
28	0.1416	["Paracentral_Lobule_L": 0.56]["Supp_Motor_Area_L": 0.37]
29	0.3363	["Cingulum_Ant_R": 0.83]["Cingulum_Mid_R": 0.15]
30	0.0000	["Temporal_Mid_L": 0.70]["Angular_L": 0.29]
31	0.3363	["Frontal_Mid_Orb_R": 0.68]["Frontal_Inf_Orb_R": 0.32]
32	0.3009	["Frontal_Inf_Oper_L": 0.43]["Precentral_L": 0.35]["Frontal_Mid_L": 0.12]
34	0.1239	["Temporal_Inf_R": 0.38]["Temporal_Mid_R": 0.34]["Temporal_Pole_Mid_R": 0.28]
35	0.0531	["Postcentral_L": 0.78]["Precentral_L": 0.21]
36	1.0088	["Temporal_Mid_L": 1.00]
37	0.1416	["Cuneus_R": 0.49]["Precuneus_R": 0.48]
38	0.1770	["Frontal_Med_Orb_R": 0.21]["Cingulum_Ant_L": 0.19]["Frontal_Med_Orb_L": 0.14]["Cingulum_Ant_R": 0.13]["Olfactory_L": 0.11]["Olfactory_R": 0.11]
39	0.4602	["Insula_L": 0.83]["Putamen_L": 0.15]
40	1.1150	["Precentral_R": 0.69]["Postcentral_R": 0.31]
41	0.2655	["Cerebelum_6_L": 0.60]["Cerebelum_4_5_L": 0.22]
42	0.5841	["Putamen_L": 0.76]["Insula_L": 0.18]
43	0.0000	["Occipital_Mid_L": 1.00]
44	0.0000	["Frontal_Mid_Orb_R": 0.57]["Frontal_Sup_Orb_R": 0.43]
45	0.1416	["Fusiform_L": 0.66]["Temporal_Inf_L": 0.21]["ParaHippocampal_L": 0.13]
46	0.0708	["Heschl_R": 0.41]["Insula_R": 0.37]["Rolandic_Oper_R": 0.20]
47	0.5487	["Cingulum_Mid_L": 0.32]["Cingulum_Mid_R": 0.26]["Cingulum_Ant_L": 0.20]["Cingulum_Ant_R": 0.18]
48	0.0531	["Temporal_Inf_R": 0.85]["Temporal_Mid_R": 0.15]
49	0.1062	["Parietal_Inf_L": 0.59]["SupraMarginal_L": 0.22]["Postcentral_L": 0.19]
50	0.0531	["None": 1.00]
51	0.3009	["Precuneus_L": 0.82]["Parietal_Sup_L": 0.18]
52	0.1416	["Temporal_Mid_R": 0.59]["Temporal_Sup_R": 0.41]

53	0.2478	["Frontal_Sup_Medial_L": 0.68]["Frontal_Sup_Medial_R": 0.23]
54	0.0177	["Paracentral_Lobule_R": 0.71]["Paracentral_Lobule_L": 0.24]
55	2.3363	["Cerebelum_6_R": 0.47]["Cerebelum_4_5_R": 0.31]["Cerebelum_10_R": 0.13]
56	1.2212	["Precentral_R": 0.77]["Frontal_Inf_Oper_R": 0.20]
57	0.1770	["Temporal_Mid_L": 1.00]
58	0.3186	["Cuneus_L": 0.46]["Calcarine_L": 0.31]["Occipital_Sup_L": 0.13]
59	0.0000	["Frontal_Sup_Medial_L": 0.42]["Frontal_Sup_L": 0.36]["Supp_Motor_Area_L": 0.21]
60	0.2655	["Cingulum_Ant_R": 0.94]
61	0.1416	["Parietal_Sup_R": 0.56]["Precuneus_R": 0.41]
62	0.2124	["Occipital_Inf_R": 0.81]["Lingual_R": 0.12]
63	0.0531	["Lingual_R": 0.49]["Calcarine_R": 0.39]
64	0.0177	["Frontal_Inf_Oper_R": 0.65]["Frontal_Inf_Tri_R": 0.34]
65	0.3717	["Temporal_Sup_L": 0.50]["SupraMarginal_L": 0.30]["Postcentral_L": 0.20]
66	0.0000	["Temporal_Mid_L": 0.58]["Temporal_Sup_L": 0.42]
67	0.0885	["Caudate_R": 0.94]
68	0.3540	["SupraMarginal_R": 0.92]
69	0.2301	["Temporal_Mid_R": 0.85]["Temporal_Sup_R": 0.15]
70	0.2301	["Fusiform_R": 0.57]["Cerebelum_6_R": 0.32]
71	0.2301	["Thalamus_R": 0.51]["None": 0.32]["Thalamus_L": 0.17]
72	0.1416	["Precentral_L": 0.69]["Frontal_Mid_L": 0.17]["Frontal_Sup_L": 0.15]
73	0.0177	["Parietal_Inf_L": 0.79]["Angular_L": 0.18]
74	0.6549	["Frontal_Inf_Tri_L": 0.84]["Frontal_Mid_L": 0.15]
75	0.0885	["Insula_R": 0.51]["Frontal_Inf_Tri_R": 0.22]["Putamen_R": 0.15]["Frontal_Inf_Orb_R": 0.12]
76	0.1416	["Lingual_R": 0.84]["Cerebelum_6_R": 0.11]
77	0.0177	["Cingulum_Mid_L": 0.94]
78	0.0885	["Cerebelum_8_L": 0.40]["Cerebelum_Crus2_L": 0.27]["Cerebelum_Crus1_L": 0.18]
80	0.2478	["Frontal_Mid_Orb_R": 0.38]["Frontal_Sup_Orb_R": 0.29]["Frontal_Sup_R": 0.25]
81	0.5133	["Postcentral_R": 0.51]["Precentral_R": 0.49]
82	0.0354	["Temporal_Pole_Sup_L": 0.50]["Temporal_Mid_L": 0.27]
83	0.0177	["Cerebelum_Crus1_R": 0.61]["Temporal_Inf_R": 0.29]
84	0.1416	["Frontal_Sup_Medial_L": 0.50]["Frontal_Sup_Medial_R": 0.39]
85	0.0531	["Hippocampus_L": 0.43]["ParaHippocampal_L": 0.40]["Fusiform_L": 0.12]
87	0.0000	["Fusiform_L": 0.46]["Temporal_Inf_L": 0.44]
88	0.1593	["Frontal_Mid_L": 0.70]["Frontal_Inf_Tri_L": 0.30]
89	0.0177	["Supp_Motor_Area_R": 0.41]["Supp_Motor_Area_L": 0.29]["Frontal_Sup_Medial_R": 0.16]["Frontal_Sup_Medial_L": 0.14]
90	0.0885	["Precentral_L": 0.57]["Postcentral_L": 0.36]
91	0.0531	["Amygdala_L": 0.42]["Hippocampus_L": 0.35]
92	0.0531	["Calcarine_R": 0.52]["Precuneus_R": 0.30]["Cuneus_R": 0.17]
93	0.2655	["Frontal_Sup_R": 0.61]["Frontal_Mid_R": 0.39]
94	0.0885	["Temporal_Mid_L": 0.56]["Temporal_Inf_L": 0.37]
95	0.1239	["Postcentral_L": 0.88]["Precentral_L": 0.12]
96	0.3363	["Frontal_Mid_R": 0.73]["Frontal_Inf_Tri_R": 0.27]

97	0.3186	["Cerebelum_9_R": 0.47]["None": 0.39]["Cerebelum_10_R": 0.11]
98	0.6903	["Thalamus_R": 0.96]
99	0.6549	["Cingulum_Mid_R": 0.54]["Cingulum_Mid_L": 0.25]["None": 0.21]
100	1.0442	["Caudate_L": 0.36]["Olfactory_L": 0.26]["Olfactory_R": 0.18]["Caudate_R": 0.14]
101	0.1593	["Temporal_Pole_Mid_R": 0.60]["Temporal_Pole_Sup_R": 0.40]
102	0.0708	["Parietal_Inf_L": 0.82]["Postcentral_L": 0.15]
103	0.4248	["Cingulum_Mid_R": 0.87]
104	0.1947	["Parietal_Sup_L": 0.55]["Precuneus_L": 0.44]
105	0.6018	["Occipital_Mid_R": 0.47]["Temporal_Mid_R": 0.44]
106	0.1239	["Frontal_Sup_L": 0.69]["Frontal_Mid_L": 0.31]
107	0.0531	["Putamen_R": 0.85]["Pallidum_R": 0.15]
108	0.0531	["Cuneus_L": 0.83]["Occipital_Sup_L": 0.17]
109	0.5310	["Cingulum_Ant_L": 0.55]["Cingulum_Ant_R": 0.45]
110	0.4248	["Temporal_Inf_R": 0.90]
111	0.0000	["Fusiform_R": 0.65]["ParaHippocampal_R": 0.31]
112	0.0177	["Temporal_Inf_L": 0.69]["None": 0.16]["Temporal_Pole_Mid_L": 0.11]
113	0.0177	["Supp_Motor_Area_R": 0.99]
114	0.0000	["Occipital_Mid_L": 0.97]
115	0.0885	["SupraMarginal_R": 1.00]
116	0.8142	["Frontal_Sup_Medial_R": 0.78]["Frontal_Sup_R": 0.22]
117	0.0177	["Postcentral_L": 0.94]
118	0.0177	["Precuneus_L": 0.77]["Cingulum_Mid_L": 0.23]
119	0.0885	["Cerebelum_Crus1_R": 0.92]
120	0.0177	["Occipital_Mid_L": 0.90]
121	0.0354	["Frontal_Inf_Orb_R": 0.77]["Frontal_Mid_Orb_R": 0.12]["Frontal_Sup_Orb_R": 0.11]
122	0.0531	["Calcarine_L": 0.59]["Lingual_L": 0.39]
123	0.4779	["Frontal_Inf_Orb_L": 0.78]["Frontal_Inf_Tri_L": 0.22]
124	0.1770	["Postcentral_R": 0.55]["Paracentral_Lobule_R": 0.35]
125	0.0708	["Putamen_R": 0.81]["Pallidum_R": 0.19]
126	0.4956	["None": 1.00]
127	0.0177	["Cerebelum_Crus1_L": 0.82]["Cerebelum_Crus2_L": 0.18]
128	0.6549	["Temporal_Mid_R": 0.54]["Temporal_Sup_R": 0.45]
129	0.0531	["Frontal_Sup_L": 0.62]["Frontal_Mid_L": 0.35]
130	0.1062	["Insula_L": 0.37]["Putamen_L": 0.35]["Temporal_Sup_L": 0.15]
131	0.1062	["Frontal_Inf_Tri_L": 0.93]
132	0.1593	["Thalamus_L": 0.50]["None": 0.25]["Hippocampus_L": 0.20]
133	0.1593	["Frontal_Inf_Tri_R": 0.82]["Frontal_Inf_Orb_R": 0.18]
134	0.0708	["Cerebelum_Crus1_R": 0.85]
135	0.0531	["Occipital_Mid_R": 0.67]["Angular_R": 0.33]
136	0.3894	["Cerebelum_Crus2_L": 0.68]["Cerebelum_Crus1_L": 0.30]
137	0.1593	["Cingulum_Post_L": 0.38]["Cingulum_Post_R": 0.25]["Cingulum_Mid_R": 0.22]
138	0.9735	["Angular_L": 0.39]["Parietal_Inf_L": 0.38]["SupraMarginal_L": 0.23]
139	0.1062	["Hippocampus_L": 0.50]["ParaHippocampal_L": 0.30]["Amygdala_L": 0.12]

140	0.0885	["Frontal_Inf_Orb_L": 0.87]["Frontal_Mid_Orb_L": 0.13]
141	0.0000	["SupraMarginal_R": 0.50]["Angular_R": 0.45]
142	0.3717	["Frontal_Sup_Medial_R": 0.93]
143	0.0531	["Temporal_Inf_R": 0.65]["Temporal_Pole_Mid_R": 0.31]
144	0.4956	["Vermis_8": 0.48]["Cerebelum_8_R": 0.32]
145	0.2478	["Precentral_L": 0.74]["Frontal_Sup_L": 0.23]
146	0.1947	["Fusiform_R": 0.68]["Lingual_R": 0.16]
147	0.2124	["Precentral_R": 0.58]["Frontal_Sup_R": 0.42]
148	0.3186	["Insula_L": 0.78]["Frontal_Inf_Oper_L": 0.18]
149	0.1593	["Rectus_L": 0.37]["Rectus_R": 0.31]["Frontal_Med_Orb_L": 0.19]["Frontal_Med_Orb_R": 0.13]
150	0.0885	["Supp_Motor_Area_R": 0.50]["Frontal_Sup_R": 0.42]
151	0.1770	["Cuneus_R": 0.55]["Occipital_Sup_R": 0.31]["Calcarine_R": 0.13]
152	1.1681	["None": 1.00]
153	1.3805	["Frontal_Mid_R": 1.00]
154	0.0885	["Frontal_Sup_L": 0.70]["Frontal_Mid_L": 0.30]
155	1.5398	["Temporal_Mid_R": 0.67]["Temporal_Inf_R": 0.33]
156	0.1770	["Cingulum_Mid_L": 0.56]["Supp_Motor_Area_L": 0.33]
157	0.3717	["Temporal_Mid_L": 0.70]["Temporal_Sup_L": 0.30]
158	0.3540	["Cingulum_Ant_L": 0.54]["Frontal_Sup_Medial_L": 0.46]
159	0.2478	["Precentral_R": 0.70]["Frontal_Mid_R": 0.30]
160	0.0177	["Frontal_Mid_L": 0.91]
161	0.4425	["Insula_L": 0.52]["Rolandic_Oper_L": 0.46]
162	0.2655	["Insula_R": 0.75]["Rolandic_Oper_R": 0.13]
163	0.2478	["Calcarine_R": 0.69]["Lingual_R": 0.25]
164	0.2478	["Angular_L": 0.79]["Parietal_Inf_L": 0.16]
165	0.3540	["Rolandic_Oper_R": 0.61]["Precentral_R": 0.23]["Postcentral_R": 0.16]
166	0.2301	["Fusiform_R": 0.41]["Hippocampus_R": 0.21]["Temporal_Inf_R": 0.20]["ParaHippocampal_R": 0.18]
167	0.6549	["Frontal_Sup_L": 0.70]["Frontal_Mid_L": 0.27]
168	0.3894	["Caudate_L": 0.42]["Putamen_L": 0.30]["Rectus_L": 0.22]
169	0.0354	["Occipital_Inf_R": 0.85]
170	0.3894	["Caudate_R": 0.37]["Olfactory_R": 0.26]["Rectus_R": 0.20]["Putamen_R": 0.13]
171	0.0000	["Paracentral_Lobule_L": 0.56]["Precuneus_L": 0.37]
172	0.4602	["Frontal_Mid_Orb_R": 0.81]["Frontal_Mid_R": 0.19]
173	0.0708	["Occipital_Inf_L": 0.89]
174	0.1062	["Frontal_Sup_R": 0.81]["Supp_Motor_Area_R": 0.19]
175	0.0354	["Cerebelum_6_L": 0.75]["Cerebelum_Crus1_L": 0.24]
176	0.1416	["Calcarine_L": 0.79]["Occipital_Sup_L": 0.11]
177	0.1416	["Calcarine_L": 0.35]["Precuneus_L": 0.28]["Lingual_L": 0.26]
178	0.4602	["Frontal_Sup_Medial_L": 0.83]["Frontal_Sup_L": 0.17]
179	0.3363	["Cerebelum_Crus1_R": 0.64]["Cerebelum_6_R": 0.22]["Cerebelum_Crus2_R": 0.12]
180	0.0885	["Lingual_R": 0.55]["Precuneus_R": 0.17]["Vermis_4_5": 0.16]
181	0.3894	["Parietal_Sup_L": 0.86]["Parietal_Inf_L": 0.14]
182	0.0177	["Temporal_Inf_L": 0.32]["Fusiform_L": 0.29]["Temporal_Pole_Mid_L": 0.25]

183	1.0619	["Occipital_Mid_R": 0.53]["Occipital_Sup_R": 0.47]
184	0.7257	["Cingulum_Ant_L": 0.39]["Cingulum_Ant_R": 0.32]["Cingulum_Mid_L": 0.27]
185	0.1062	["Thalamus_L": 0.54]["Thalamus_R": 0.46]
186	0.2301	["Frontal_Mid_L": 0.80]["Precentral_L": 0.20]
187	0.1239	["Precentral_L": 0.61]["Postcentral_L": 0.39]
188	0.0177	["Fusiform_L": 0.80]["Cerebelum_4_5_L": 0.14]
189	0.6726	["Angular_L": 0.92]
190	0.2478	["Frontal_Sup_R": 0.82]["Frontal_Sup_Medial_R": 0.18]
191	0.3363	["Frontal_Inf_Oper_R": 0.72]["Frontal_Inf_Tri_R": 0.13]
192	0.2832	["Frontal_Mid_R": 0.51]["Frontal_Inf_Tri_R": 0.36]["Frontal_Inf_Orb_R": 0.13]
193	0.0708	["Precuneus_L": 0.74]["Precuneus_R": 0.22]
194	0.7611	["Postcentral_R": 0.74]["Precentral_R": 0.19]
195	0.7257	["Cerebelum_6_R": 0.49]["Cerebelum_4_5_R": 0.40]
196	0.1770	["None": 0.93]
197	0.0000	["Temporal_Mid_L": 0.98]
198	0.0000	["Frontal_Inf_Tri_L": 0.64]["Frontal_Mid_L": 0.36]
199	0.4425	["Postcentral_R": 0.50]["SupraMarginal_R": 0.47]
200	0.3186	["Cingulum_Mid_R": 0.65]["Precuneus_R": 0.16]["Paracentral_Lobule_R": 0.12]
201	0.0885	["Frontal_Inf_Orb_R": 0.49]["Insula_R": 0.41]
202	0.0354	["Frontal_Mid_Orb_L": 0.77]["Frontal_Mid_L": 0.14]
203	0.0177	["Fusiform_L": 0.45]["Hippocampus_L": 0.20]["Temporal_Inf_L": 0.20]["ParaHippocampal_L": 0.15]
204	0.2124	["Cerebelum_Crus2_L": 0.52]["Cerebelum_Crus1_L": 0.48]
205	0.0177	["Temporal_Pole_Sup_R": 0.58]["Temporal_Pole_Mid_R": 0.36]
206	0.2832	["SupraMarginal_L": 0.54]["Parietal_Inf_L": 0.46]
207	0.3717	["Parietal_Inf_R": 0.63]["Angular_R": 0.37]
208	1.1504	["Hippocampus_R": 0.44]["Precuneus_R": 0.27]
209	0.4779	["Temporal_Mid_R": 0.93]
210	0.5133	["Temporal_Sup_L": 0.44]["Rolandic_Oper_L": 0.30]["Temporal_Pole_Sup_L": 0.20]
211	0.4956	["Precuneus_L": 0.44]["Cuneus_L": 0.28]["Occipital_Sup_L": 0.17]["Parietal_Sup_L": 0.11]
212	0.2478	["Frontal_Mid_R": 0.96]
213	0.1062	["None": 0.66]["Vermis_1_2": 0.15]
214	0.1770	["Frontal_Inf_Tri_L": 0.84]["Frontal_Inf_Oper_L": 0.16]
215	0.2478	["Frontal_Mid_L": 0.56]["Precentral_L": 0.44]
216	0.0531	["Postcentral_R": 0.62]["Parietal_Sup_R": 0.38]
217	0.0000	["Temporal_Mid_L": 0.90]
218	0.4248	["Temporal_Mid_R": 1.00]
219	0.0177	["Occipital_Mid_L": 1.00]
220	0.2655	["Postcentral_R": 0.78]["Precentral_R": 0.22]
221	0.4956	["Frontal_Inf_Orb_L": 0.80]["Temporal_Pole_Sup_L": 0.18]
222	0.2832	["Frontal_Mid_R": 0.50]["Precentral_R": 0.46]
223	0.0000	["Cingulum_Mid_R": 0.63]["Supp_Motor_Area_R": 0.37]
224	0.1770	["Insula_R": 0.61]["Temporal_Sup_R": 0.17]
225	0.1770	["Lingual_R": 0.51]["Cerebelum_Crus1_R": 0.38]

226	0.6903	["Cingulum_Ant_L": 0.81]["Frontal_Sup_Medial_L": 0.18]
227	0.5664	["Cerebelum_6_R": 0.89]
228	0.1416	["Temporal_Mid_R": 0.69]["Temporal_Inf_R": 0.31]
229	0.0177	["Occipital_Sup_R": 0.69]["Cuneus_R": 0.31]
230	0.5841	["Cerebelum_9_L": 0.64]["Cerebelum_10_L": 0.36]
231	0.1593	["Fusiform_L": 0.42]["Lingual_L": 0.30]["Cerebelum_6_L": 0.21]
232	0.9558	["Frontal_Med_Orb_R": 0.73]["Frontal_Sup_Orb_R": 0.14]["Rectus_R": 0.13]
233	0.1239	["Thalamus_L": 1.00]
234	0.1947	["Temporal_Mid_L": 0.50]["Occipital_Mid_L": 0.49]
235	0.1062	["Frontal_Sup_L": 0.98]
236	0.2655	["Temporal_Pole_Sup_R": 0.31]["Insula_R": 0.26]["Frontal_Inf_Orb_R": 0.19]
237	0.0531	["Parietal_Inf_L": 1.00]
238	0.0354	["Amygdala_L": 0.37]["Putamen_L": 0.32]["Hippocampus_L": 0.16]
239	0.4602	["Cingulum_Mid_R": 0.48]["Cingulum_Mid_L": 0.38]["None": 0.14]
240	0.2832	["Precuneus_R": 0.71]["Parietal_Sup_R": 0.17]["Precuneus_L": 0.13]
241	0.0000	["Frontal_Sup_R": 0.59]["Frontal_Mid_R": 0.38]
242	0.2301	["None": 0.45]["Lingual_R": 0.22]["Thalamus_R": 0.19]
243	0.3009	["Temporal_Mid_L": 0.70]["Temporal_Sup_L": 0.30]
244	0.0885	["Paracentral_Lobule_L": 0.46]["Supp_Motor_Area_R": 0.17]["Cingulum_Mid_L": 0.12]["Paracentral_Lobule_R": 0.11]
245	0.3894	["None": 0.51]["Thalamus_L": 0.22]["Thalamus_R": 0.16]
246	0.2478	["Insula_R": 0.54]["Temporal_Sup_R": 0.21]["Putamen_R": 0.13]
247	0.0177	["Cerebelum_9_L": 0.40]["None": 0.31]["Vermis_10": 0.21]
248	0.0177	["Precuneus_R": 0.72]["Cingulum_Mid_R": 0.20]
249	0.1239	["Frontal_Sup_L": 0.62]["Frontal_Mid_L": 0.38]
250	0.4602	["Postcentral_R": 0.30]["Rolandic_Oper_R": 0.27]["Temporal_Sup_R": 0.26]["SupraMarginal_R": 0.16]
251	0.2301	["Temporal_Inf_L": 0.58]["Temporal_Mid_L": 0.42]
252	0.4071	["Angular_R": 0.96]
253	0.2832	["Vermis_6": 0.40]["Cerebelum_6_L": 0.37]
254	0.1239	["Frontal_Sup_L": 0.41]["Frontal_Sup_Orb_L": 0.33]["Frontal_Mid_Orb_L": 0.24]
255	0.0000	["Frontal_Sup_Medial_R": 0.66]["Frontal_Sup_R": 0.32]
256	0.3363	["Cingulum_Mid_R": 0.89]
257	0.0708	["Postcentral_L": 0.79]["Parietal_Sup_L": 0.21]
258	0.6195	["Cerebelum_6_R": 0.75]["Cerebelum_Crus1_R": 0.12]["Cerebelum_8_R": 0.11]
259	0.0708	["Temporal_Inf_R": 0.84]
260	0.3009	["Frontal_Inf_Orb_L": 0.63]["Insula_L": 0.18]
261	0.2655	["SupraMarginal_L": 0.81]["Postcentral_L": 0.19]
262	0.0885	["ParaHippocampal_L": 0.57]["Cerebelum_4_5_L": 0.35]
263	0.0708	["Occipital_Mid_L": 0.47]["Occipital_Sup_L": 0.39]
264	0.3009	["Frontal_Med_Orb_L": 0.83]["Rectus_L": 0.15]
265	0.6903	["Frontal_Inf_Tri_R": 0.93]
266	0.0708	["Frontal_Mid_L": 1.00]
267	0.7080	["Cerebelum_3_R": 0.53]["Cerebelum_4_5_R": 0.19]["ParaHippocampal_R": 0.13]

268	0.1239	["Thalamus_L": 0.47]["Hippocampus_L": 0.25]["Lingual_L": 0.18]
269	0.1416	["Cuneus_R": 0.78]["Cuneus_L": 0.18]
270	0.3009	["Temporal_Sup_R": 1.00]
271	0.5133	["Temporal_Pole_Sup_L": 0.56]["Temporal_Sup_L": 0.30]["Temporal_Mid_L": 0.15]
272	0.4248	["Parietal_Inf_R": 0.59]["SupraMarginal_R": 0.41]
273	0.0531	["Frontal_Inf_Orb_R": 0.99]
274	0.0885	["Insula_L": 0.54]["Rolandic_Oper_L": 0.44]
275	0.5841	["Precuneus_R": 0.86]["Precuneus_L": 0.14]
276	0.1239	["Cerebelum_4_5_L": 0.66]["Cerebelum_3_L": 0.19]["None": 0.14]
277	0.2478	["Temporal_Inf_R": 0.65]["Fusiform_R": 0.35]
278	0.0354	["Fusiform_L": 0.35]["Temporal_Inf_L": 0.23]["Cerebelum_6_L": 0.19]["Occipital_Inf_L": 0.16]
279	0.1416	["Frontal_Mid_L": 0.88]
280	0.1062	["Temporal_Mid_L": 0.96]
281	0.2301	["Precentral_R": 0.87]["Frontal_Sup_R": 0.11]
282	0.0000	["Fusiform_L": 0.47]["Lingual_L": 0.45]
283	1.1858	["Cingulum_Ant_L": 0.68]["Frontal_Med_Orb_L": 0.27]
284	0.1416	["Hippocampus_R": 0.58]["ParaHippocampal_R": 0.35]
285	0.1239	["Frontal_Mid_R": 1.00]
286	0.1947	["Calcarine_L": 0.35]["Vermis_6": 0.16]
287	0.1062	["Parietal_Sup_R": 0.75]["Parietal_Inf_R": 0.13]
288	0.0177	["Temporal_Pole_Sup_R": 0.72]["Insula_R": 0.15]
289	0.8319	["Frontal_Sup_Medial_R": 0.82]["Frontal_Sup_R": 0.18]
290	0.0885	["Temporal_Inf_R": 0.62]["Temporal_Mid_R": 0.38]
291	0.2832	["Supp_Motor_Area_L": 0.61]["Supp_Motor_Area_R": 0.39]
292	0.3540	["Putamen_L": 0.27]["Pallidum_L": 0.22]["None": 0.11]
293	0.4425	["Precentral_L": 0.74]["Frontal_Inf_Oper_L": 0.26]
294	0.6903	["Occipital_Mid_R": 0.68]["Temporal_Mid_R": 0.32]
295	0.3186	["Vermis_4_5": 0.54]["Cerebelum_4_5_R": 0.26]["Cerebelum_4_5_L": 0.14]
296	0.0000	["Fusiform_L": 0.53]["Temporal_Inf_L": 0.39]
297	0.0177	["Frontal_Sup_Medial_L": 0.89]["Frontal_Sup_L": 0.11]
298	0.0531	["Temporal_Pole_Sup_L": 0.72]["Insula_L": 0.12]
299	0.0531	["Hippocampus_R": 0.63]["ParaHippocampal_R": 0.24]
300	0.2124	["Vermis_3": 0.37]["Vermis_1_2": 0.23]["Cerebelum_3_R": 0.20]
301	0.0885	["Cerebelum_Crus2_L": 0.52]["Cerebelum_Crus1_L": 0.46]
302	0.5487	["Temporal_Sup_R": 0.55]["SupraMarginal_R": 0.27]["Rolandic_Oper_R": 0.18]
303	0.4248	["Cingulum_Mid_L": 0.67]["Supp_Motor_Area_L": 0.33]
304	0.1416	["Precentral_R": 0.44]["Frontal_Mid_R": 0.29]["Frontal_Sup_R": 0.26]
305	0.4779	["Temporal_Sup_L": 0.39]["Rolandic_Oper_L": 0.33]["Postcentral_L": 0.18]
306	0.0354	["Frontal_Sup_R": 0.53]["Frontal_Mid_R": 0.47]
307	0.0531	["Insula_R": 0.68]["Putamen_R": 0.24]
308	0.1947	["Occipital_Mid_R": 0.53]["Occipital_Sup_R": 0.47]
309	0.1416	["ParaHippocampal_R": 0.46]["Hippocampus_R": 0.39]["None": 0.15]
310	0.6726	["None": 0.40]["Cerebelum_4_5_R": 0.38]["Cerebelum_3_R": 0.19]

312	0.1062	["Temporal_Inf_L": 0.93]
313	0.0000	["Temporal_Pole_Mid_R": 0.52]["ParaHippocampal_R": 0.19]["Fusiform_R": 0.15]["Temporal_Inf_R": 0.13]
314	0.1062	["SupraMarginal_L": 0.60]["Temporal_Sup_L": 0.30]
315	0.1770	["Cerebelum_9_L": 0.63]["Cerebelum_8_L": 0.21]["Vermis_9": 0.12]
316	0.1239	["Supp_Motor_Area_L": 0.99]
317	0.0708	["Rolandic_Oper_R": 0.48]["Temporal_Sup_R": 0.35]["Heschl_R": 0.17]
318	0.0177	["Occipital_Inf_L": 0.35]["Cerebelum_Crus1_L": 0.34]["Lingual_L": 0.23]
319	0.1062	["Temporal_Mid_L": 0.96]
320	0.0000	["Frontal_Inf_Tri_R": 0.56]["Frontal_Mid_R": 0.44]
321	0.1593	["Vermis_7": 0.38]["Cerebelum_Crus2_R": 0.27]["Cerebelum_Crus1_R": 0.18]
322	0.1770	["Fusiform_R": 0.64]["Cerebelum_6_R": 0.28]
323	0.3540	["Parietal_Inf_R": 0.45]["Parietal_Sup_R": 0.32]["Postcentral_R": 0.21]
324	0.5487	["Calcarine_R": 0.53]["Calcarine_L": 0.35]
325	0.3894	["Frontal_Med_Orb_R": 0.39]["Cingulum_Ant_R": 0.38]["Frontal_Sup_Medial_R": 0.22]
326	0.2655	["Occipital_Sup_L": 0.71]["Occipital_Mid_L": 0.26]
327	0.2832	["Precuneus_R": 0.62]["Cuneus_R": 0.25]
328	0.2124	["None": 0.32]["Hippocampus_R": 0.23]["ParaHippocampal_R": 0.18]["Amygdala_R": 0.12]["Pallidum_R": 0.12]
329	0.5133	["Temporal_Sup_R": 0.37]["Temporal_Mid_R": 0.33]["Temporal_Pole_Sup_R": 0.25]
330	0.0000	["Fusiform_R": 0.63]["ParaHippocampal_R": 0.25]
331	0.9027	["Temporal_Sup_L": 0.63]["Rolandic_Oper_L": 0.13]["Heschl_L": 0.12]
332	0.0885	["Lingual_L": 0.59]["Cerebelum_6_L": 0.29]
333	0.1239	["ParaHippocampal_R": 0.49]["None": 0.33]["Hippocampus_R": 0.18]
334	0.0531	["Frontal_Sup_L": 0.67]["Supp_Motor_Area_L": 0.30]
335	0.4602	["Cerebelum_Crus1_R": 0.76]
336	0.0354	["Temporal_Sup_R": 0.54]["Rolandic_Oper_R": 0.33]["Temporal_Pole_Sup_R": 0.11]
337	0.0000	["Hippocampus_L": 0.70]["ParaHippocampal_L": 0.22]
338	0.0531	["Frontal_Inf_Orb_R": 0.81]["Temporal_Pole_Sup_R": 0.13]
339	0.6372	["Putamen_L": 0.83]["Pallidum_L": 0.17]
340	0.0000	["Occipital_Sup_L": 0.56]["Occipital_Mid_L": 0.29]["Cuneus_L": 0.15]
341	0.1593	["Temporal_Mid_R": 0.46]["Temporal_Sup_R": 0.30]["Angular_R": 0.16]
342	0.0177	["Calcarine_R": 0.30]["Calcarine_L": 0.23]["Cuneus_R": 0.16]["Cuneus_L": 0.13]["Precuneus_R": 0.12]
343	1.0796	["Temporal_Mid_L": 0.67]["Temporal_Pole_Mid_L": 0.18]["Temporal_Inf_L": 0.13]
344	0.1593	["Postcentral_R": 0.45]["SupraMarginal_R": 0.34]["Parietal_Inf_R": 0.16]
345	0.3894	["Precentral_L": 0.94]
346	0.0708	["Temporal_Inf_L": 0.40]["Cerebelum_Crus1_L": 0.36]["Fusiform_L": 0.14]
347	0.0531	["Insula_R": 0.57]["Putamen_R": 0.19]["Frontal_Inf_Oper_R": 0.16]
348	0.0885	["Calcarine_R": 0.52]["Lingual_R": 0.40]
349	0.2478	["Cerebelum_9_R": 0.66]["Vermis_9": 0.26]
350	0.0708	["Cerebelum_4_5_L": 0.30]["Cerebelum_3_L": 0.24]["None": 0.20]["ParaHippocampal_L": 0.14]
351	0.3540	["Lingual_L": 0.48]["Calcarine_L": 0.46]
352	0.0708	["Supp_Motor_Area_L": 0.58]["Supp_Motor_Area_R": 0.34]
353	0.0531	["Calcarine_L": 0.51]["Cuneus_L": 0.44]

354	0.4071	["Frontal_Inf_Oper_R": 0.49]["Frontal_Inf_Tri_R": 0.27]["Frontal_Mid_R": 0.14]
355	0.1593	["Precuneus_L": 0.67]["Precuneus_R": 0.33]
356	0.2124	["Parietal_Inf_R": 0.66]["Angular_R": 0.33]
357	0.5310	["Cerebelum_Crus2_R": 0.59]["Cerebelum_Crus1_R": 0.41]
359	0.0177	["Precentral_R": 0.50]["Postcentral_R": 0.50]
360	0.1947	["Parietal_Inf_L": 0.44]["Parietal_Sup_L": 0.30]["Postcentral_L": 0.26]
361	0.6195	["Fusiform_R": 0.70]["Cerebelum_4_5_R": 0.21]
362	0.0000	["Occipital_Inf_L": 0.74]["Occipital_Mid_L": 0.25]
363	0.0531	["Temporal_Sup_L": 0.73]["SupraMarginal_L": 0.24]
364	0.4602	["Temporal_Mid_R": 0.87]["Temporal_Sup_R": 0.13]
365	0.1416	["Caudate_R": 0.84]["Thalamus_R": 0.13]
366	0.1947	["Temporal_Pole_Sup_L": 0.30]["Insula_L": 0.29]["Frontal_Inf_Orb_L": 0.25]
367	0.1947	["Occipital_Mid_R": 1.00]
368	0.0354	["Precuneus_L": 0.49]["Cingulum_Mid_L": 0.29]["Cingulum_Post_L": 0.22]
370	0.1062	["Frontal_Inf_Oper_L": 0.71]["Rolandic_Oper_L": 0.14]["Precentral_L": 0.12]
371	0.0354	["Frontal_Sup_Medial_L": 0.59]["Frontal_Sup_Medial_R": 0.24]["Cingulum_Mid_R": 0.12]
372	0.4602	["Fusiform_R": 0.48]["Lingual_R": 0.30]["Cerebelum_6_R": 0.17]
373	0.2478	["Caudate_L": 0.79]["Putamen_L": 0.15]
374	0.1416	["Temporal_Mid_L": 0.76]["Temporal_Inf_L": 0.24]
375	0.0000	["Putamen_R": 0.43]["Amygdala_R": 0.30]["Pallidum_R": 0.24]
376	0.0885	["Parietal_Sup_R": 0.62]["Occipital_Sup_R": 0.17]["Precuneus_R": 0.13]
377	0.1062	["Cerebelum_6_L": 0.60]["Cerebelum_4_5_L": 0.38]
378	0.4956	["Lingual_R": 0.32]["Lingual_L": 0.27]["Vermis_4_5": 0.23]
379	0.0354	["Frontal_Mid_L": 0.95]
380	0.1062	["Cingulum_Mid_R": 0.82]["Supp_Motor_Area_R": 0.18]
381	0.2832	["Parietal_Sup_L": 0.82]["Parietal_Inf_L": 0.18]
383	0.4602	["Temporal_Mid_R": 0.64]["Temporal_Sup_R": 0.36]
384	0.0000	["Cerebelum_Crus1_L": 0.91]
385	0.0177	["Frontal_Mid_Orb_L": 0.80]["Frontal_Inf_Orb_L": 0.12]
386	0.3363	["Frontal_Sup_R": 0.56]["Frontal_Mid_R": 0.44]
387	0.0531	["Frontal_Mid_R": 0.85]["Frontal_Sup_R": 0.15]
388	0.0177	["Temporal_Pole_Mid_L": 0.73]["Temporal_Inf_L": 0.18]
389	0.1947	["Paracentral_Lobule_R": 0.44]["Precuneus_L": 0.18]["Precuneus_R": 0.15]
391	0.2478	["Cerebelum_4_5_R": 0.52]["Lingual_R": 0.17]["ParaHippocampal_R": 0.15]["Cerebelum_3_R": 0.13]
392	0.5841	["Frontal_Sup_Medial_L": 0.81]["Frontal_Sup_L": 0.19]
393	0.0177	["Supp_Motor_Area_R": 0.81]
394	0.0177	["Temporal_Sup_L": 0.68]["Insula_L": 0.32]
395	0.0708	["Temporal_Mid_R": 0.76]["Temporal_Sup_R": 0.14]
396	0.0177	["Olfactory_R": 0.23]["Temporal_Pole_Sup_R": 0.23]["ParaHippocampal_R": 0.18]["Putamen_R": 0.11]
397	0.3717	["Frontal_Mid_R": 1.00]
398	0.2478	["Thalamus_R": 0.98]
399	0.2655	["None": 1.00]
400	0.3717	["Frontal_Mid_L": 0.88]["Frontal_Sup_L": 0.12]